Table 1. The sequences of gene-specific primers for reverse transcriptase–polymerase chain reaction (RT-PCR) and real-time RT-PCR used in this study

Primer	Sequence
IL-4 forward	CACAGGCACAAGCAGCTGAT
IL-4 reverse	CCTTCACAGGACAGGAATTCAAG
IL-6 forward	GTAGCCGCCCCACACAGA
IL-6 reverse	CCGTCGAGGATGTACCGAAT
IL-10 forward	GCCAAGCCTTGTCTGAGATGA
IL-10 reverse	CTTGATGTCTGGGTCTTGGTTCT
IL-17 forward	GACTCCTGGGAAGACCTCATTG
IL-17 reverse	TGTGATTCCTGCCTTCACTATGG
IL-17F forward	GCTTGACATTGGCATCATCAA
IL-17F reverse	GGAGCGGCTCTCGATGTTAC
IL-23 forward	GAGCCTTCTCTGCTCCCTGATAG
IL-23 reverse	AGTTGGCTGAGGCCCAGTAG
IL-23R forward	AACAACAGCTCGGCTTTGGTATA
IL-23R reverse	GGGACATTCAGCAGTGCAGTAC
IFNG forward	CATCCAAGTGATGGCTGAACTG
IFNG reverse	TCGAAACAGCATCTGACTCCTTT
GM-CSF forward	CAGCCCTGGAGCATGTG
GM-CSF reverse	CATCTCAGCAGCAGTGTCTCTAC^{r}
RORγt forward	TGGGCATGTCCCGAGATG
RORγt reverse	GCAGGCTGTCCCTCTGCTT
STAT-3 forward	GGAGGAGGCATTCGGAAAGT
STAT-3 reverse	GCGCTACCTGGGTCAGCTT
FOXP3 forward	GAGAAGCTGAGTGCCATGCA
FOXP3 reverse	GCCACAGATGAAGCCTTGGT

IL, interleukin; *IFNG*, interferon γ; *FOXP3*, forkhead box protein 3; *GM-CSF*, granulocyte–macrophage colony-stimulating factor; *RORγt*, retinoic acid receptor-related orphan receptor γ isoform t; *STAT*, signal transducer and activator of transcription.

transcribed and labelled using One-Cycle Target Labeling and Control Reagents as instructed by the manufacturer (Affymetrix, Santa Clara, CA). The labelled probes were hybridized to a Human Genome U133 Plus 2·0 Array (Affymetrix). The arrays were used in a single experiment and analysed with GENECHIP operating software 1.2 (Affymetrix). Background subtraction and normalization were performed using GENESPRING GX 7.3 software (Agilent Technologies, Santa Clara, CA). The signal intensity was pre-normalized based on the positive control genes (GAPDH and β-actin) for all measurements on that chip. To account for differences in detection efficiency between spots, the pre-normalized signal intensity of each gene was normalized to the median of pre-normalized measurements for that gene. The data were filtered as follows. (i) Genes that were scored as absent in all samples were eliminated. (ii) Genes with a signal intensity of < 90 were eliminated. (iii) Genes that exhibited increased (fold-change > 2) or decreased (fold-change > 2) expression in CB-derived $CD4^+$ T cells compared with PB-derived $CD4^+$ T cells were selected by comparing the mean value of signal intensities in each condition.

Immunofluorescence study

After periods of cultivation, cells were collected and stained with fluorescence-labelled monoclonal antibodies and analysed by flow cytometry (FC500; Beckman/Coulter, Fullerton, CA). A four-colour immunofluorescence study was performed with a combination of fluorescein isothiocyanate (FITC)-conjugated anti-CD3, phycoerythrin (PE)-conjugated anti- forkhead box protein 3 (Foxp3), phycoerythrin-cyanine-5 (PC5)-conjugated anti-CD4 and PC7-conjugated anti-CD8 (Beckman/Coulter). After staining of cell surface antigens, cells were permeabilized with IntraPrep (Dako, Glostrup, Denmark) and intracellular antigen (Foxp3) was further stained.

Statistical analysis

The statistical analysis was performed using a Student's *t*-test and a *P*-value < 0·05 was considered to be statistically significant.

Results

Expression profiles of activated $CD4^+$ T cells derived from human CB and PB

To compare the gene expression patterns of CB-derived $CD4^+$ cells and PB-derived $CD4^+$ cells, we performed DNA microarray analysis using the Affymetrix Human Genome U133 Plus 2·0 Array. After background subtraction, comparison of the gene expression profiles of two independent CB-derived $CD4^+$ samples and PB-derived $CD4^+$ samples was performed using a gene cluster analysis. The genes differentially expressed (fold-change > 2) between the activated $CD4^+$ T cells derived from CB and those derived from PB were selected, and 396 probes were found to exhibit higher levels of expression in CB-derived $CD4^+$ samples while 131 probes exhibited higher levels in PB-derived $CD4^+$ samples. Parts of the data are summarized and presented in Fig. 1a and Tables 2–4.

Among these genes, those closely correlated to T-cell function and development were selected (Fig. 1b). The genes exhibiting higher levels of expression in CB-derived $CD4^+$ samples included those encoding cell cycle regulators, including cyclin-dependent kinase (CDKN)2A and 2B, transcriptional regulators and signal transduction factors (Tables 2 and 3). The genes for cytokines, chemokines and their receptors such as Interferon γ (IFNG), granulocyte-macrophage colony-stimulating factor (GM-CSF) and for T-cell transcriptional regulators (*FOXP3*) as well as the genes related to T-cell development including CD28, cytotoxic T lymphocyte antigen-4 (CTLA4) and inducible T-cell co-stimulator (ICOS) were also found among the genes exhibiting higher levels of expression in CB-derived $CD4^+$ samples (Fig. 1b). The factors reported

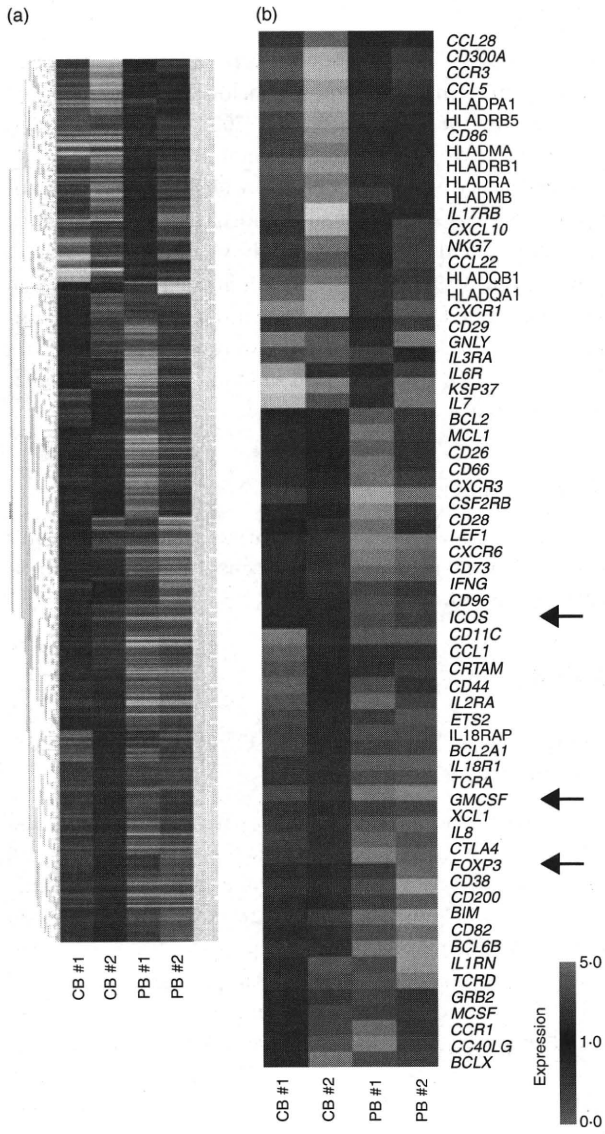

Figure 1. Comparison of the gene expression profiles of cord blood (CB)- and peripheral blood (PB)-derived $CD4^+$ T cells. Hierarchical clustering of results from a microarray analysis for CB- and PB-derived $CD4^+$ T cells is indicated. (a) A total of 529 genes characterizing $CD4^+$ T cells (396 genes for CB-derived $CD4^+$ T cells and 131 genes for PB-derived $CD4^+$ T cells) were used to create the gene tree. The gene list is presented in Tables 3 and 4. (b) Genes related to T-cell development (40 genes for CB-derived $CD4^+$ T cells and 26 genes for PB-derived $CD4^+$ T cells) are presented. The arrows indicate the expression pattern of T-cell lineage-specific genes including inducible T-cell co-stimulator (*ICOS*), granulocyte-macrophage colony-stimulating factor (*GM-CSF*) and forkhead box protein 3 (*FOXP3*).

to be essential for negative selection in $CD4^+$ $CD8^+$ thymocytes such as BCL2-like 11 (BIM)[10] as well as other apoptotic regulators were also found among the genes exhibiting higher expression levels in CB-derived $CD4^+$ samples.

The genes with a higher level of expression in the PB-derived $CD4^+$ T cells included those encoding transcriptional regulators, signal transduction factors, major histocompatibility complex (MHC) class II molecules (*HLADMA*, *HLADMB*, *HLADPA1*, *HLADQB1*, *HLADRA*, *HLADRB1* and *HLADRB5*), and cytokines, chemokines and their receptors (*IL-7*, *IL-17RB*), as well as genes that characterize the T-cell lineage (*CD29*, *CD86*) (Fig. 1b, Tables 2, 4).

Notably, microarray studies showed that the expression of several regulatory T cell (Treg)-related genes was significantly higher in the CB-derived T cells. Foxp3 is an important T-cell transcription factor and is considered to be a marker of Tregs. Cytotoxic T-lymphocyte antigen-4 (CTLA-4) and ICOS, which belong to the CD28 family of receptors and play a crucial role in the activation of T cells, were reported to be highly expressed in activated Tregs.[11,12] All of the above genes were expressed at higher levels in the CB-derived CD4 T cells (Fig. 1).

The microarray results for major genes related to the development of the T-cell lineage, including those not appeared in Fig. 1, are summarized in Table 2. As shown in Table 2, the expression of T-cell lineage master regulator genes, such as *TBX21*, *GATA3* and *MAF*, and T cell-related cytokines, such as *IL-4*, *IL-5*, *IL-13*, *IL-22* and *TGFB1*, revealed no significant difference between CB-derived $CD4^+$ cells and PB-derived $CD4^+$ cells. However, other T cell-related genes, including *IL-2*, *IL-6*, *IL-9*, *IL-10* and *IL-17*, were eliminated from the list in the course of background subtraction because the signal intensity of each gene was low (< 90 as raw data) in all of the samples.

Differences in the expression patterns of T-cell lineage-specific genes between CB-derived and PB-derived $CD4^+$ T cells

To further confirm the characteristic gene expression in CB- and PB-derived $CD4^+$ T cells, we performed a real-time RT-PCR analysis. Consistent with the microarray data, when the mRNA levels of the genes related to the T helper type 1 (Th1) and Th2 phenotypes were examined, higher levels of GM-CSF and IFNG were observed in CB-derived T cells, while IL-4 revealed no significant tendency (Fig. 2). We also examined IL-6 and IL-10 and no significant tendency was observed either in the expression of these genes (Fig. 2).

Next we examined the expression of the genes related to Tregs and observed a higher level of Foxp3, but lower levels of retinoic acid receptor-related orphan receptor γ isoform t (RORγt); and IL-17F, in CB-derived T cells (Fig. 3). In contrast, there was no significant tendency in the expression of genes encoding signal transducer and activator of transcription 3 (STAT-3), IL-23 and IL-23 receptors. In the case of the *IL-17* gene, clear amplifica-

Table 2. The microarray results for T-cell-related genes

			CB-I		CB-2		PB-1		PB-2	
Description	Gene	Gene ID	Normalized	Raw	Normalized	Raw	Normalized	Raw	Normalized	Raw
Master regulation										
Thl	*TBX21*	220684_at	1·1382915	305·7	0·7851455	247·1	1·045663	230·5	0·954337	261·4
Th2	*GATA3*	209602_s_at	1·471558	1204	0·7742825	742·1	1·0740323	721·1	0·9259675	772·5
	GATA3	209603_at	1·265932	416·5	0·53335179	205·7	1·0535141	284·5	0·9464856	317·6
	GATA3	209604_s_at	1·350573	5300	0·6415387	2950	1·0573606	3406	0·9426395	3773
	MAF	206363_at	0·7447395	672·7	0·8744312	925·6	1·1255689	834·5	1·2704437	1170
	MAF	209348_s_at	1·0320604	2078	0·8329663	1965	0·9679398	1600	1·8301903	3758
	MAF	229327_s_at	0·9099149	569·7	0·6089576	446·8	1·090085	560·2	1·4076804	898·9
Treg	*FOXP3*	221334_s_at	1·8893701	100·6	1·4199468	88·6	0·4988136	21·8	0·5800531	31·5
	FOXP3	224211_at	1·6205869	152·3	1·4101433	155·3	0·5898568	45·5	0·2347433	22·5
Cytokines										
Thl	*IFNG*	210354_at	1·4801383	2000	1·9182948	3037	0·457517	507·4	0·5198616	716·4
	GM-CSF	210229_s_at	1·2802086	1293	2·6726868	3163	0·6906437	572·5	0·7197912	741·4
Th2	*IL-4*	207538_at	2·0291064	687·2	0·3361219	133·4	0·9317174	259	1·0682826	369
	IL-4	207539_s_at	2·8263247	965	0·3561467	142·5	0·8481774	237·7	1·1518226	401·1
	IL-5	207952_at	1·3380713	810	0·0610382	43·3	1·0097023	501·7	0·9902797	611·4
	IL-13	207844_at	3·9835246	1712	0·8117443	408·8	1·1453367	404	0·8691162	452·9
Treg	*TGFB1*	203085_s_at	1·5166419	774·9	0·9012154	539·6	1·0987847	460·8	0·8546632	374·6
Others	*IL-22*	222974_at	0·1272062	5·2	4·325279	207·2	0·5632869	18·9	1·4367131	59·9
Surface molecules										
Treg	*CTLA4*	231794_at	1·3871489	336·9	1·2560804	357·5	0·7439196	148·3	0·4444751	110·1
	CTLA4	236341_at	1·2573498	905·7	1·6210791	1368	0·6800935	402·1	0·7426501	545·6
Others	*IL-2RA*	206341_at	1·5216751	3569	1·2715347	3494	0·7284654	1402	0·6569936	1571
	IL-2RA	211269_s_at	1·1563299	4436	1·3173387	5923	0·8436702	2657	0·560745	2194
	ICOS	210439_at	1·378036	619·8	1·343834	708·3	0·567216	209·4	0·656166	301
	CD28	211856_x_at	1·3887135	144·9	1·2905376	157·8	0·3292731	28·2	0·7094624	75·5
	CD28	211861_x_at	1·350062	183·3	1·4109998	224·5	0·4863549	54·2	0·649938	90

The microarray results for major genes related to the development of the T-cell lineage are summarized. The normalized and raw data for four samples are indicated for each gene. Those for which differential expression was found between cord blood (CB)- and peripheral blood (PB)-derived $CD4^+$ T cells in a gene cluster analysis (fold-change > 2) are highlighted in grey. Genes exhibiting low signal intensity (< 90 as raw data) in all of the four samples were eliminated from the list beforehand in the process of background subtraction, and thus do not appeared in this table.

CTLA-4, cytotoxic T-lymphocyte antigen-4; *FOXP3*, forkhead box protein 3; GATA, GATA family of zinc finger trancription factors; *GM-CSF*, granulocyte–macrophage colony-stimulating factor; ICOS, inducible T-cell co-stimulator; IFNG, interferon γ; *IL*, interleukin; MAF, macrophage-activating factor; TBX21, T-box protein 21; TGFB1, transforming growth factor, beta 1; Th1, T helper type 1; Treg, regulatory T cell.

tion was detected in PB-derived T cells whereas no amplification was observed in the samples of CB-derived T cells (data not shown).

To further investigate whether increased expression of the *FOXP3* gene is a general feature of CB-derived $CD4^+$ T cells, we tested four samples of CB-derived $CD4^+$ T cells by real-time RT-PCR analysis and compared the results with those for equivalent numbers of PB-derived samples. As shown in Fig. 4, two CB-derived samples (CB 4 and 5, at 2 weeks) revealed significantly increased gene expression of *FOXP3* when compared with PB-derived samples, whereas the remaining two samples (CB 3 and 6; termed 'additional' samples below) did not. We also tested *FOXP3* gene expression at an earlier time-point in the same samples and observed no significant increase of *FOXP3* gene expression in CB-derived $CD4^+$ T cells at 1 week (Fig. 4). When the data were analysed statistically, expression of the *FOXP3* gene was found to be significantly higher in CB-derived $CD4^+$ T cells in comparison with equivalent PB-derived $CD4^+$ T cells at both 1 week ($P < 0{\cdot}05$) and 2 weeks ($P < 0{\cdot}05$) (Fig. 4).

Next we assessed the expression of the Foxp3 protein in CB-derived $CD4^+$ T cells. When the same samples as described above were examined by flow cytometry using a specific antibody, the Foxp3 protein was certainly detected in a portion of cells in all of four CB-derived samples while not detected in any of the PB-derived samples tested (Fig. 5). Inconsistent with the results of real-time RT-PCR, expression level of Foxp3 proteins was higher in CB-derived $CD4^+$ T cells at 1 week than at 2 weeks.

Table 3. Genes up-regulated in $CD4^+$ T cells from cord blood samples 1 and 2 (CB 1 and CB 2, respectively)

		Fold change				
Affi ID	Gene abbreviation	CB 1	CB 2	PB 1	PB 2	Gene name
Apoptosis						
1555372_at	*BimL*	1·39	1·52	0·61	0·42	BCL2-like 11 (apoptosis facilitator)
237837_at	*BCL2*	1·27	1·32	0·49	0·73	B-cell CLL/lymphoma 2
205681_at	*BCL2A1*	1·91	1·53	0·39	0·47	BCL2-related protein A1
1558143_a_at	*BCL2L11*	1·68	1·74	0·32	0·32	BGL2-like 11 (apoptosis facilitator)
228311_at	*BCL6B*	1·36	3·39	0·64	0·26	B-cell CLL/lymphoma 6, member B (zinc finger protein)
215037_s_at	*BCLX*	2·56	1·27	0·73	0·56	BCL2-like 1
224414_s_at	*CARD6*	2·65	1·34	0·56	0·66	Caspase recruitment domain family, member 6
201631_s_at	*IER3*	1·62	2·95	0·38	0·31	Immediate early response 3
218000_s_at	*PHLDA1*	2·34	1·21	0·53	0·79	Pleckstrin homology-like domain, family A, member 1
209803_s_at	*PHLDA2*	2·87	1·32	0·31	0·68	Pleckstrin homology-like domain, family A. member 2
203063_at	*PPMIF*	1·26	1·53	0·74	0·64	Protein phosphatase IF (PP2C domain containing)
205214_at	*STK17B*	1·78	1·26	0·74	0·71	Serine/threonine kinase 17b (apoptosis-inducing)
217853_at	*TENS1*	1·63	6·00	0·04	0·37	Tensin 1
B- and T-cell development						
211861_x_at	*CD28*	1·35	1·41	0·49	0·65	CD28 antigen(Tp44)
207892_at	*CD40LG*	3·67	1·32	0·45	0·68	C040 ligand (TNF superfamily, member 5, hyper-IgM syndrome)
206914_at	*CRTAM*	2·76	1·60	0·40	0·36	Class I MHC-restricted T-cell-associated molecule
210557_x_at	*CSF1*	3·79	1·22	0·78	0·70	Colony-stimulating factor 1 (macrophage)
210229_s_at	*CSF2*	1·28	2·67	0·69	0·72	Colony-stimulating factor 2 (granulocyte–macrophage)
205159_at	*CSF2RB*	2·33	1·60	0·18	0·40	Colony-stimulating factor 2 receptor
231794_at	*CTLA4*	1·39	1·26	0·74	0·44	Cytotoxic T-lymphocyte-associated protein 4
204232_at	*FCER1G*	1·63	2·14	0·28	0·37	Fc fragment of IgE, high affinity 1, receptor for; gamma polypeptide
210439_at	*ICOS*	1·38	1·34	0·57	0·66	Inducible T-cell costimulator
210354_at	*IFNG*	1·48	1·92	0·46	0·52	Human mRNA for HuIFN -gamma interferon
230536_at	*PBX4*	1·48	1·26	0·50	0·74	Pre-B-cell leukaemia transcription factor 4
215540_at	*TCRA*	1·25	1·87	0·67	0·75	T-cell antigen receptor alpha
234440_al	*TCRD*	7·51	1·48	0·50	0·52	Human T-cell receptor delta-chain
Cell growth and maintenance						
213497_at	*ABTB2*	2·06	1·34	0·66	0·63	Ankyrin repeat and BTB (POZ) domain containing 2
201236_s_at	*BTG2*	1·60	1·23	0·60	0·77	BTG family, member 2
235287_at	*CDK6*	1·50	1·32	0·44	0·68	Cyclin-dependent kinase 6
209644_x_at	*CDKN2A*	2·90	1·21	0·67	0·79	Cyclin-dependent kinase inhibitor 2A (melanoma, p16, inhibits CDK4)
236313_at	*CDKN2B*	3·24	1·28	0·58	0·72	Cyclin-dependent kinase inhibitor 2B (p15, inhibits CDK4)
241984_at	*CHES1*	1·38	1·34	0·66	0·63	Checkpoint suppressor 1
202552_s_at	CRIM1	1·94	1·39	0·32	0·61	Cysteine-rich transmembrane BMP regulator 1 (chordin-like)
204844_at	*ENPEP*	1·64	1·75	0·09	0·36	Glutamyl aminopeptidase (aminopeptidase A)
205418_at	*FES*	1·39	1·80	0·61	0·25	Feline sarcoma oncogene
228572_at	*GRB2*	4·69	1·21	0·79	0·78	Growth factor receptor-bound protein 2
207688_s_at	*INHBC*	1·46	1·25	0·51	0·75	Inhibin, beta C
209744_x_at	*ITCH*	1·30	1·47	0·63	0·70	Itchy homolog E3 ubiquitin protein ligase (mouse)
201548_s_at	*JARID1B*	1·27	1·92	0·73	0·46	Jumonji, AT-rich interactive domain IB (RBP2-like)
203297_s_at	*JARID2*	1·42	1·28	0·54	0·72	Jumonji, AT-rich interactive domain 2
41387_r_at	*JMJD3*	1·82	1·24	0·76	0·65	Jumonji domain containing 3
205569_at	*LAMP3*	2·32	1·24	0·76	0·50	Lysosomal-associated membrane protein 3
214039_s_at	*LAPTM4B*	1·41	1·49	0·49	0·59	Lysosomal-associated protein transmembrane 4 beta
205857_x_at	*MSH3*	1·79	1·28	0·58	0·72	MutS homolog 3 (*E. coli*)
209550_at	*NDN*	3·42	1·38	0·17	0·62	Necdin homolog (mouse)
207943_x_at	*PLAGL1*	1·37	1·43	0·57	0·63	Pleiomorphic adenoma gene-like 1
204748_at	*PTGS2*	1·65	1·78	0·14	0·35	Prostaglandin-endoperoxide synthase 2
201482_at	*QSCN6*	1·32	1·23	0·38	0·77	Quiescin Q6
203743_s_at	*TDG*	1·47	1·23	0·54	0·77	Thymine-DNA glycosylase
204227_s_at	*TK2*	2·12	1·26	0·56	0·74	Thymidine kinase 2, mitochondrial

Table 3. Continued

Affi ID	Gene abbreviation	Fold change CB 1	CB 2	PB 1	PB 2	Gene name
Cytokines and chemokines						
207533_at	*CCL1*	1·67	1·48	0·52	0·49	Chemokine (C-C motif) ligand 1
205099_s_at	*CCR1*	4·70	1·21	0·61	0·79	Chemokine (C-C motif) receptor 1
207681_at	*CXCR3*	1·51	1·33	0·41	0·67	Chemokine (C-X-C motif) receptor 3
211469_s_at	*CXCR6*	1·58	1·95	0·32	0·42	Chemokine (C-X-C motif) receptor 6
206613_at	*IL-18R1*	2·32	1·38	0·61	0·62	Interleukin-18 receptor 1
207072_at	*IL-18RAP*	2·16	1·44	0·46	0·56	Interleukin-18 receptor accessory protein
212657_s_at	*IL-1RN*	1·44	3·12	0·56	0·37	Interleukin 1 receptor
206341_at	*IL-2RA*	1·52	1·27	0·73	0·66	Interleukin-2 receptor alpha
202859_x_at	*IL-8*	1·31	3·75	0·38	0·69	Interleukin-8
202643_s_at	*TNFAIP3*	1·61	1·25	0·67	0·75	Tumour necrosis factor, alpha-induced protein 3
202687_s_at	*TNFSF10*	2·83	1·23	0·67	0·77	Tumour necrosis factor (ligand) superfamily member 10
205599_at	*TRAF1*	2·25	1·32	0·68	0·61	Tumour necrosis factor receptor-associated factor 1
202871_at	*TRAF4*	1·43	1·58	0·57	0·48	Tumour necrosis factor receptor-associated factor 4
206366_x_at	*XCL1*	1·24	2·66	0·46	0·76	Chemokine (C motif) ligand 1
Signal transduction						
210538_s_at	*AIP1*	1·35	1·54	0·65	0·61	Baculoviral IAP repeat-containing 3
209369_at	*ANXA3*	1·39	6·82	0·61	0·05	Annexin A3
1554343_a_at	*BRDG1*	1·45	1·67	0·52	0·55	BCR downstream signalling 1
225946_at	*C12orf2*	3·20	1·77	0·23	0·23	Ras association (RaIGDS/AF-6) domain family 8
204392_at	*CAMK1*	1·26	1·62	0·74	0·54	Calcium/calmodulin-dependent protein kinase I
231042_s_at	*CAMK2D*	1·31	1·63	0·25	0·69	Calcium/calmodulin-dependent protein kinase (CaM kinase) II delta
205692_s_at	*CD38*	1·37	1·29	0·71	0·48	CD38 antigen (p45)
231747_at	*CYSLTR1*	3·16	1·45	0·55	0·43	Cysteinyl leukotriene receptor 1
211272_s_at	*DGKA*	1·43	1·23	0·77	0·54	Diacylglycerol kinase alpha 80 kDa
200762_at	*DPYSL2*	1·35	1·40	0·37	0·65	Dihydropyrimtdinase-like 2
208370_s_at	*DSCR1*	1·23	1·90	0·63	0·77	Down syndrome critical region gene 1
204794_at	*DUSP2*	1·55	2·57	0·39	0·45	Dual specificity phosphatase 2
204015_s_at	*DUSP4*	1·35	2·66	0·65	0·39	Dual specificity phosphatase 4
211333_s_at	*FASLG*	1·20	1·37	0·49	0·80	Fas ligand (TNF superfamily, member 6)
211535_s_at	*FGFR1*	1·23	2·79	0·70	0·77	Fibroblast growth factor receptor 1
224148_at	*FYB*	1·50	1·21	0·45	0·79	FYN binding protein (FYB-120/130)
209304_x_at	*GADD45B*	1·55	1·29	0·65	0·71	Growth arrest and DNA-damage-inducible beta
234284_at	*GNG8*	1·50	3·16	0·50	0·35	Guanine nucleotide binding protein (G protein), gamma 8
224285_at	*GPR174*	1·91	1·42	0·56	0·58	G protein-coupled receptor 174
223767_at	*GPR84*	4·41	1·44	0·05	0·56	G protein-coupled receptor 84
211555_s_at	*GUCY1B3*	1·66	1·73	0·34	0·03	Guanylate cyclase 1, soluble, beta 3
38037_at	*HBEGF*	1·54	1·36	0·55	0·64	Heparin-binding EGF-like growth factor
203820_s_at	*IMP-3*	1·83	2·18	0·17	0·17	IGF-II-mRNA-binding protein 3
203006_at	*INPP5A*	1·40	1·86	0·60	0·52	Inositol polyphosphate-5-phosphatase, 40 kDa
231779_at	*IRAK2*	1·93	1·46	0·46	0·54	Interleukin-1 receptor associated kinase 2
32137_at	*JAG2*	1·58	1·29	0·71	0·64	Jagged 2
203904_x_at	*KAI1*	1·65	1·59	0·41	0·25	CD82 antigen
235252_at	*KSR*	1·72	1·56	0·43	0·44	Kinase suppressor of ras 1
210948_s_at	*LEF1*	1·21	1·64	0·41	0·79	Hypothetical protein LOC641518
203236_s_at	*LGALS9*	1·48	1·27	0·73	0·51	Lectin, galactoside-binding, soluble, 9 (galectin 9)
220253_s_at	*LRP12*	1·27	1·30	0·31	0·73	Low-density lipoprotein-related protein 12
206637_at	*P2RY14*	1·32	1·48	0·39	0·68	Purinergic receptor P2Y, G-protein coupled, 14
210837_s_at	*PDE4D*	1·35	1·31	0·62	0·69	Phosphodiesterase 4D, cAMP-specific
206726_at	*PGDS*	6·45	1·40	0·60	0·43	Prostaglandin D2 synthase, haematopoietic
210617_at	*PHEX*	1·53	4·08	0·21	0·47	Phosphate regulating endopeptidase homologue, X-linked
206370_at	*PIK3CG*	1·23	1·32	0·50	0·77	Phosphoinositide-3-kinase, catalytic, gamma polypeptide
205632_s_at	*PIP5K1B*	1·32	1·42	0·64	0·68	Phosphalidylinositol-4-phosphate 5-kinase, type 1 beta

Table 3. Continued

Affi ID	Gene abbreviation	Fold change CB 1	CB 2	PB 1	PB 2	Gene name
215195_at	*PRKCA*	2·17	1·36	0·64	0·61	Protein kinase C, alpha
210832_x_at	*PTGER3*	4·44	1·47	0·07	0·53	Prostaglandin E receptor 3 (subtype EP3)
1553535_a_at	*RANGAP1*	1·58	1·39	0·58	0·61	Ran GTPase activating protein 1
234344_at	*RAP2C*	1·75	1·26	0·46	0·74	RAP2C, member of RAS oncogene family
223809_at	*RGS18*	2·12	1·67	0·15	0·33	Regulator of G-protein signalling 18
209882_at	*RIT1*	1·74	1·32	0·63	0·68	Ras-like without CAAX 1
209451_at	*TANK*	1·34	1·20	0·42	0·80	TRAF family member-associated NFKB activator
204924_at	*TLR2*	1·60	2·52	0·36	0·40	Toll-like receptor 2
217979_at	*TM4SF13*	1·21	2·47	0·30	0·79	Tetraspanin 13
209263_x_at	*TM4SF7*	2·05	1·41	0·58	0·59	Tetraspanin 4
Transcription						
1566989_at	*ARID1B*	1·42	1·27	0·09	0·73	AT-rich interactive domain 1B (SWIl-like)
203973_s_at	*CEBPD*	3·06	1·51	0·33	0·49	CCAAT/enhancer binding protein (C/EBP), delta
221598_s_at	*CRSP8*	1·60	1·29	0·71	0·68	Cofactor required for Spl transcriptional activation, subunit 8, 34 kDa
205249_at	*EGR2*	1·33	4·27	0·67	0·60	Early growth response 2 (Krox-20 homologue, *Drosophila*)
206115_at	*EGR3*	1·31	6·15	0·69	0·48	Early growth response 3
201328_at	*ETS2*	1·57	1·72	0·43	0·40	V-ets erythroblastosis virus E26 oncogene homologue 2 (avian)
218810_at	*FLJ23231*	2·13	1·37	0·63	0·63	Zinc finger CCCH-type containing 12A
209189_at	*FOS*	21·56	1·31	0·13	0·69	V-fos FBJ murine osteosarcoma viral oncogene homologue
223408_s_at	*FOXK2*	2·26	1·22	0·48	0·78	Forkhead box K2
202723_s_at	*FOXO1A*	1·47	1·27	0·57	0·73	Forkhead box O1A (rhabdomyosarcoma)
224211_at	*FOXP3*	1·62	1·41	0·59	0·23	Forkhead box P3
207156_at	*HIST1H2AG*	1·73	1·30	0·41	0·70	Histone 1, H2ag
220042_x_at	*HIVEP3*	1·26	1·65	0·74	0·56	Human immunodeficiency virus type I enhancer binding protein 3
207826_s_at	*ID3*	1·34	8·64	0·60	0·66	Inhibitor of DNA binding 3, dominant negative helix-loop-hetix protein
204549_at	*IKBKE*	2·33	1·29	0·71	0·66	Inhibitor of kappa light polypeptide gene enhancer in B cells
219878_s_at	*KLF13*	1·89	1·26	0·34	0·74	Kruppel-like factor 13
207667_s_at	*MAP2K3*	1·33	1·28	0·72	0·57	Mitogen-activated protein kinase kinase 3
201502_s_at	*NFKBIA*	2·31	1·29	0·71	0·57	Nuclear factor of κ light polypeptide gene enhancer in B cells inhibitor
222105_s_at	*NKIRAS2*	1·84	1·21	0·69	0·79	NFKB inhibitor interacting Ras-like 2
204622_x_at	*NR4A2*	1·35	4·31	0·65	0·63	Nuclear receptor subfamily 4, group A, member 2
207978_s_at	*NR4A3*	1·33	3·53	0·62	0·67	Nuclear receptor subfamily 4, group A, member 3
202600_s_at	*NRIPI*	1·86	1·39	0·26	0·61	Nuclear receptor interacting protein 1
216841_s_at	*SOD2*	1·25	1·73	0·36	0·75	Superoxide dismutase 2, mitochondrial
201416_at	*SOX4*	1·53	2·21	0·47	0·38	SRY (sex determining region Y)-box 4
223635_s_at	*SSBP3*	2·12	1·25	0·75	0·62	Single-stranded DNA binding protein 3
206506_s_at	*SUPT3H*	1·47	1·31	0·57	0·69	Suppressor of Ty 3 homologue (*S. cerevisiae*)
221618_s_at	*TAF9L*	1·25	1·49	0·47	0·75	TAF9-like RNA polymerase II
203177_x_at	*TFAM*	1·63	1·23	0·77	0·57	Transcription factor A, mitochondrial
213943_at	*TWIST1*	1·89	3·14	0·04	0·11	Twist homologue 1 (acrocephalosyndactyly 3; Saethre-Chotzen syndrome)
219836_at	*ZBED2*	1·33	4·76	0·67	0·21	Zinc finger, BED-type containing 2
211965_at	*ZFP36L1*	2·02	1·47	0·29	0·53	Zinc finger protein 36, C3H type-like 1
230760_at	*ZFY*	1·41	1·25	0·75	0·02	Zinc finger protein, Y-linked
228854_at	*ZNF145*	3·26	1·21	0·40	0·79	Transcribed locus
235121_at	*ZNF542*	2·68	1·33	0·63	0·67	Zinc finger protein 542

To investigate whether increased expression of the *IL-17* gene is a general feature of PB-derived $CD4^+$ T cells, we also tested *IL-17* gene expression in the above-described additional samples by real-time RT-PCR analysis. As shown in Fig. 6, all of four PB-derived $CD4^+$ T-cell samples revealed significantly increased gene expression of *IL-17* when compared with the CB-derived samples at 1 week. At 2 weeks, however, *IL-17* gene expression in PB-derived $CD4^+$ T cells was diminished while some of the CB-derived $CD4^+$ T cells (such as sample CB 4) exhibited increased *IL-17* gene expression. When the data were analysed statistically, expression of the *IL-17* gene was found to be

Table 4. Genes up-regulated in $CD4^+$ T cells from peripheral blood (PB)

Affi ID	Gene abbreviation	Fold change				Gene name
		CB 1	CB 2	PB 1	PB 2	
Apoptosis						
1553681_a_at	*PRF1*	0·66	0·51	1·41	1·34	Perforin 1 (pore-forming protein)
B- and T-cell development						
224499_s_at	*AICDA*	0·06	0·44	1·56	3·47	Activation-induced cytidine deaminase
205495_s_at	*GNLY*	0·40	0·51	1·49	6·34	Granulysin
217478_s_at	*HLA-DMA*	0·67	0·39	1·33	1·35	Major histocompatibility complex, class II, DM alpha
203932_at	*HLA-DMB*	0·64	0·31	2·02	1·36	Major histocompatibility complex, class II, DM beta
211991_s_at	*HLA-DPA1*	0·50	0·14	1·54	1·50	Major histocompatibility complex, class II, DP alpha 1
212671_s_at	*HLA-DQA1*	0·44	0·23	1·56	2·56	Major histocompatibility complex, class II, DQ alpha 1
211656_x_at	*HLA-DQB1*	0·63	0·48	1·37	7·07	Major histocompatibility complex, class II, DQ beta 1
210982_s_at	*HLA-DRA*	0·58	0·37	1·50	1·42	Major histocompatibility complex, class II, DR alpha
208306_x_at	*HLA-DRB1*	0·51	0·24	1·49	1·61	Major histocompatibility complex, class II, DR beta 3
204670_x_at	*HLA-DRB5*	0·63	0·22	1·47	1·37	Major histocompatibility complex, class II, DR beta 5
211634_x_at	*IGHV1-69*	0·69	0·77	1·23	1·99	Immunoglobulin heavy variable 1–69
211645_x_at	*IgK*	0·15	0·49	1·51	6·62	Immunoglobulin kappa light chain (IGKV)
221651_x_at	*IGKC*	0·46	0·68	1·32	5·57	Immunoglobulin kappa constant
215379_x_at	*IGLC2*	0·62	0·41	1·38	4·26	Immunoglobulin lambda joining 2
209031_at	*IGSF4*	0·50	0·03	2·33	1·50	Immunoglobulin superfamily, member 4
205686_s_at	*CD86*	0·70	0·23	1·30	1·39	CD86 antigen (CD28 antigen ligand 2, B7-2 antigen)
204698_at	*ISG20*	0·68	0·49	1·32	1·64	Interferon stimulated exonuclease gene, 20 kDa
213915_at	*NKG7*	0·72	0·42	1·28	2·31	Natural killer cell group 7 sequence
Cell growth and maintenance						
201334_s_at	*ARHGEF12*	0·74	0·50	1·26	1·96	Rho guanine nucleotide exchange factor (GEF) 12
230292_at	*CHC1L*	0·70	0·56	1·30	2·02	Regulator of chromosome condensation (RCC1)
205081_at	*CRIP1*	0·56	0·73	1·27	1·75	Cysteine-rich protein 1 (intestinal)
31874_at	*GAS2L1*	0·77	0·52	1·23	2·35	Growth arrest-specific 2 like 1
202364_at	*MXI1*	0·43	0·73	1·27	1·44	MAX interactor 1
219304_s_at	*PDGFD*	0·65	0·71	1·29	3·68	Platelet-derived growth factor D
213397_x_at	*RNASE4*	0·64	0·46	1·36	2·21	Ribonuclease, RNase A family, 4
213566_at	*RNASE6*	0·69	0·39	1·49	1·31	Ribonuclease, RNase A family, k6
219077_s_at	*WWOX*	0·40	0·78	1·25	1·22	WW domain containing oxidoreductase
Cytokine and chemokine						
207861_at	*CCL22*	0·76	0·52	1·24	2·47	Chemokine (C–C motif) ligand 22
238750_at	*CCL28*	0·74	0·45	1·26	1·41	Chemokine (C–C motif) ligand 28
1555759_a_at	*CCL5*	0·71	0·23	1·29	1·92	Chemokine (C–C motif) ligand 5
208304_at	*CCR3*	0·50	0·12	1·50	2·35	Chemokine (C–C motif) receptor 3
205898_at	*CX3CR1*	0·30	0·20	1·70	4·16	Chemokine (C–X3–C motif) receptor 1
204533_at	*CXCL10*	0·80	0·16	1·20	2·53	Chemokine (C–X–C motif) ligand 10
219255_x_at	*IL-17RB*	0·73	0·04	1·27	1·29	Interleukin 17 receptor B
206148_at	*IL-3RA*	0·60	0·54	2·46	1·40	Interleukin 3 receptor, alpha (low affnity)
226333_at	*IL-6R*	0·22	0·79	1·21	2·43	Interleukin-6 receptor
206693_at	*IL-7*	0·09	0·54	1·46	5·86	Interleukin-7
Signal transduction						
204497_at	*ADCY9*	0·76	0·40	1·24	2·40	Adenylate cyclase 9
206170_at	*ADRB2*	0·58	0·35	1·42	3·97	Adrenergic, beta-2-, receptor, surface
202096_s_at	*BZRP*	0·50	0·54	1·59	1·46	Benzodiazapine receptor (peripheral)
230464_at	*EDG8*	0·04	0·09	1·91	2·42	Endothelial differentiation, sphingolipid G-protein-coupled receptor 8
223423_at	*GPR160*	0·54	0·68	1·40	1·32	G protein-coupled receptor 160
227769_at	*GPR27*	0·07	0·08	1·92	244	G protein in-coupled receptor 27
210095_s_at	*IGFBP3*	0·27	0·20	1·73	5·25	Insulin-like growth factor binding protein 3
38671_at	*PLXND1*	0·08	0·65	1·35	2·57	Plexin D1
226101_at	*PRKCE*	0·56	0·43	1·72	1·44	Protein kinase C. epsilon
232629_at	*PROK2*	0·01	0·13	1·87	2·09	Prokineticin 2

Table 4. Continued

Affi ID	Gene abbreviation	Fold change CB 1	CB 2	PB 1	PB 2	Gene name
203329_at	*PTPRM*	0·36	0·62	1·38	1·93	Protein tyrosine phosphatase, receptor type, M
204731_at	*TGFBR3*	0·78	0·55	1·22	2·04	Transforming growth factor, beta receptor III (betaglycan, 300 kDa)
Transcription						
203129_s_at	*KIF5C*	0·67	0·09	1·33	3·43	Kinesin family member 5C
213906_at	*MYBL1*	0·75	0·51	1·25	3·63	V-myb myeloblastosis viral oncogene homologue (avian)-like 1
209815_at	*PTCH*	0·59	0·27	1·41	4·17	Patched homologue (*Drosophila*)
213891_s_at	*TCF4*	0·74	0·65	2·06	1·26	Transcription factor 4
238520_at	*TRERFI*	0·70	0·77	1·23	2·30	Transcriptional regulating factor 1
203603_s_at	*ZFHX1B*	0·74	0·61	1·26	3·63	Zinc finger homobox 1b
213218_at	*ZNF187*	0·74	0·69	1·26	1·76	Zinc finger protein 187
221123_x_at	*ZNF395*	0·38	0·71	1·63	1·29	Zinc finger protein 395

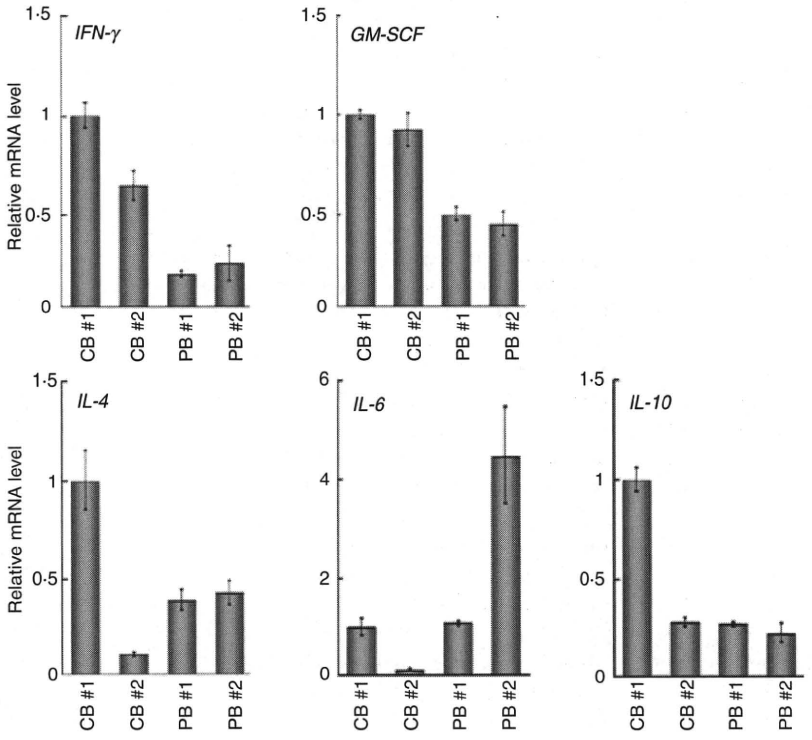

Figure 2. Quantitative polymerase chain reaction (PCR) analysis of the genes related to the T helper type 1 (Th1) and Th2 phenotypes. The expression of the genes indicated was examined by real-time reverse transcriptase (RT)-PCR using the same sample specimens as in Fig 1. Data are normalized to the mRNA level in PB 1 which is arbitrarily set to 1. The signal intensity was normalized using that of a control housekeeping gene [the human glyceraldehyde-3-phosphate dehydrogenase (*GAPDH*) gene]. Data are relative values with the standard deviation (SD) for triplicate wells.

significantly higher in PB-derived $CD4^+$ T cells in comparison with equivalent CB-derived $CD4^+$ T cells at 1 week ($P < 0{\cdot}05$) but not at 2 weeks (Fig. 6).

Discussion

Although it is generally believed that there are functional differences between CB and PB lymphocytes, the details are obscure. For instance, Azuma *et al.*[13] reported that the phenotype and function of expanded CB lymphocytes were essentially equivalent to those of expanded PB lymphocytes when evaluated in *in vitro* experiments. In the present study, however, we have shown that CB-derived $CD4^+$ T cells revealed a distinct expression profile of genes important for the function of particular T-cell subsets compared with PB-derived $CD4^+$ T cells.

$CD4^+$ T cells can be classified into distinct subsets, including effector $CD4^+$ cells and Tregs, according to their functional characteristics as well as differentiation profiles.[14–16] Typically, effector $CD4^+$ T cells have been further divided into two distinct lineages on the basis of their cytokine production profiles, namely Th1 and Th2. Th1 cells producing cytokines such as IL-2, IFN-γ and GM-CSF have evolved to enhance the eradication of intracellular pathogens and are thought to be potent activators of cell-mediated immunity. In contrast, Th2

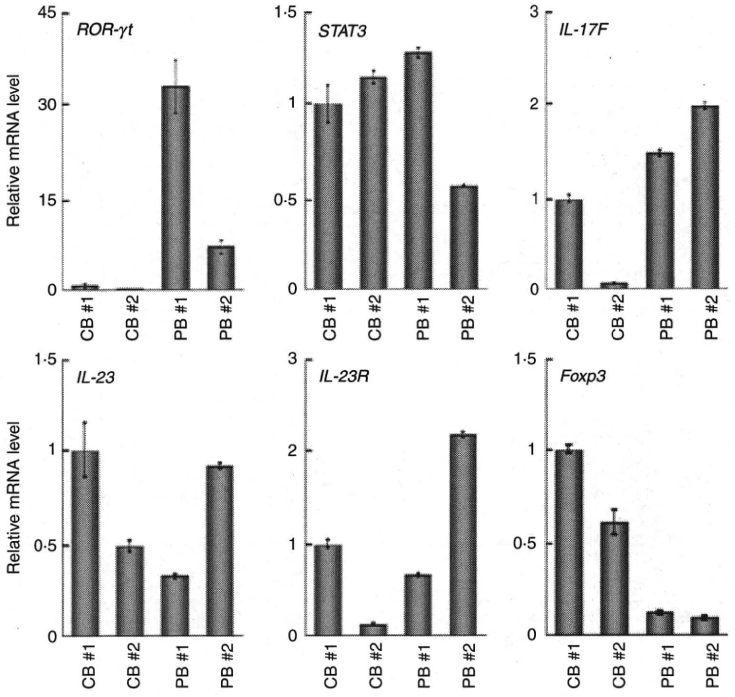

Figure 3. Quantitative polymerase chain reaction (PCR) analysis of the forkhead box protein 3 gene (*FOXP3*) and the genes related to the secretion of interleukin (IL)-17. The expression of the genes indicated was examined as in Fig 2. Data are normalized to the mRNA level in peripheral blood sample 1 (PB 1) as in Fig.2. The signal intensity was normalized using that of a control housekeeping gene [the human glyceraldehyde-3-phosphate dehydrogenase (*GAPDH*) gene]. Data are relative values with the standard deviation for triplicate wells.

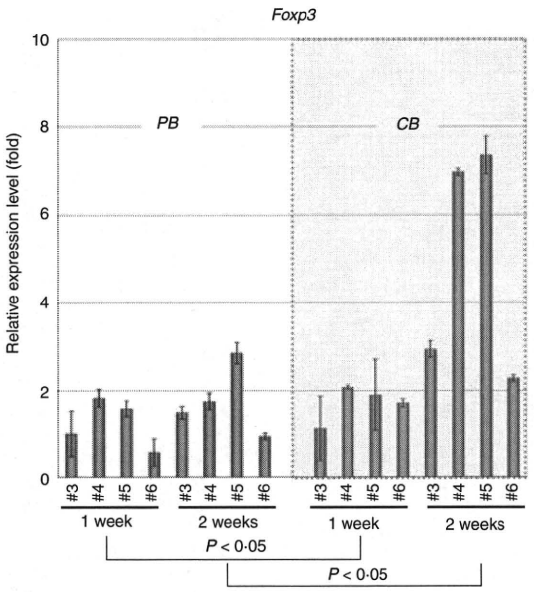

Figure 4. Quantitative polymerase chain reaction (PCR) analysis of the forkhead box protein 3 gene (*FOXP3*) in additional samples. Additional peripheral blood (PB) and cord blood (CB) samples were prepared and RNAs were extracted at 1 and 2 weeks. The expression of the *FOXP3* gene was examined as in Fig. 2. Data are normalized to the mRNA level in the sample of PB 3 at 1 week, which is arbitrarily set to 1. The signal intensity was normalized using that of a control housekeeping gene (the human β-actin gene). Data are relative values with the standard deviation for triplicate wells. The data were analysed statistically and *FOXP3* gene expression in CB-derived $CD4^+$ T cells was found to be significantly higher in comparison with equivalent PB-derived $CD4^+$ T cells at both 1 week ($P < 0{\cdot}05$) and 2 weeks ($P < 0{\cdot}05$).

cells secreting cytokines such as IL-4, IL-5, IL-6, IL-9 and IL-13 have evolved to enhance the elimination of parasitic infections and are thought to be potent activators of B-cell immunoglobulin E production, eosinophil recruitment, and mucosal expulsion. Th1-type responses to self or commensal floral antigens can promote tissue destruction and chronic inflammation, whereas dysregulated Th2-type responses can cause allergy and asthma. The development of Th1 is specified by the transcription factor T-bet (also known as Tbx-21) and master regulators of Th2 differentiation are GATA-3 and c-maf.

As shown in Fig. 2 and Table 2, the gene expression profiles of CB- and PB-derived $CD4^+$ T cells revealed no significant differences regarding cytokines related to the definition of Th1 and Th2, with the exceptions of IFN-γ and GM-CSF. The mRNA levels of IFN-γ and GM-CSF tended to be higher in CB-derived $CD4^+$ T cells than in PB-derived $CD4^+$ T cells. The mRNA expression of the transcription factors T-bet, GATA-3 and c-maf, which regulate Th1 and Th2 cell differentiation, did not differ significantly between CB- and PB-derived $CD4^+$ T cells.

In addition to Th1 and Th2 cells, IL-17 (also known as IL-17A)-producing T lymphocytes have been recently shown to comprise a distinct third subset of T helper cells, termed Th17 cells, in the mouse immune system. Th17 cells exhibit pro-inflammatory characteristics and act as major contributors to autoimmune disease. A number of experiments using animal models support a significant role for IL-17 in the response to allografts.[14,16,17] There is as yet no direct evidence for the existence of discrete Th17 cells in humans, although

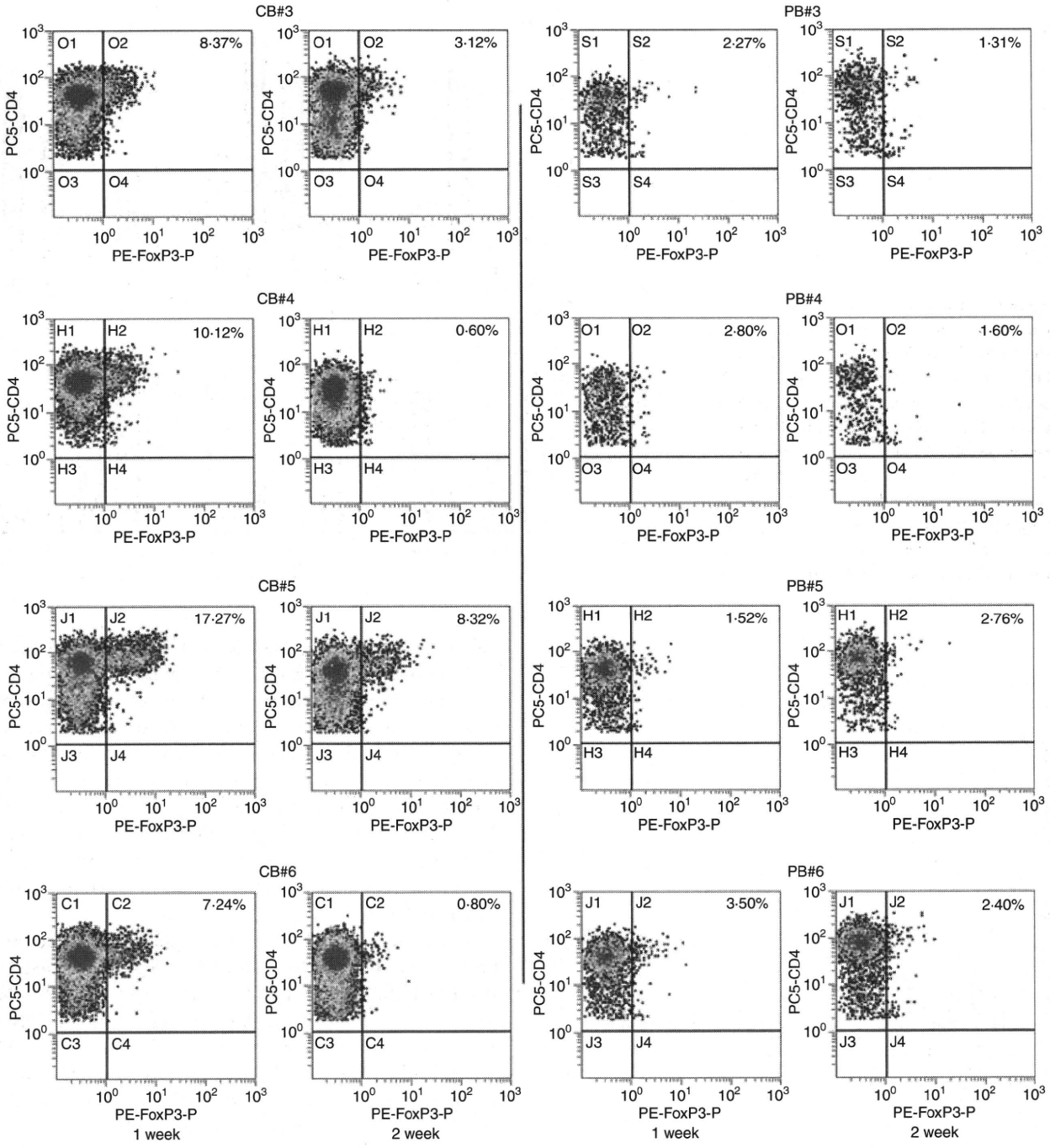

Figure 5. Protein expression of forkhead box protein 3 (Foxp3) in activated $CD4^+$ T cells. The protein expression of Foxp3 in same sample specimens as in Fig. 4 was examined by flow cytometry. The CD4 versus Foxp3 cytogram of the population gated with $CD3^+$ and $CD4^+$ in each sample is presented.

helper T cells secreting IL-17 have clearly been detected in the human immune system.[18] Several studies have shown a correlation between allograft rejection and IL-17. For example, IL-17 levels are elevated in human renal allografts during subclinical rejection and there are detectable mRNA levels in the urinary mononuclear cell sediments of these patients.[19,20] In human lung organ transplantation, IL-17 levels have also been reported to be elevated during acute rejection.[21] Interestingly, in this study, most of the PB-derived $CD4^+$ T-cell samples expressed higher levels of IL-17 mRNA than the CB-derived $CD4^+$ T-cell samples, suggesting that PB-derived $CD4^+$ T cells frequently include potent IL-17-secreting T cells.

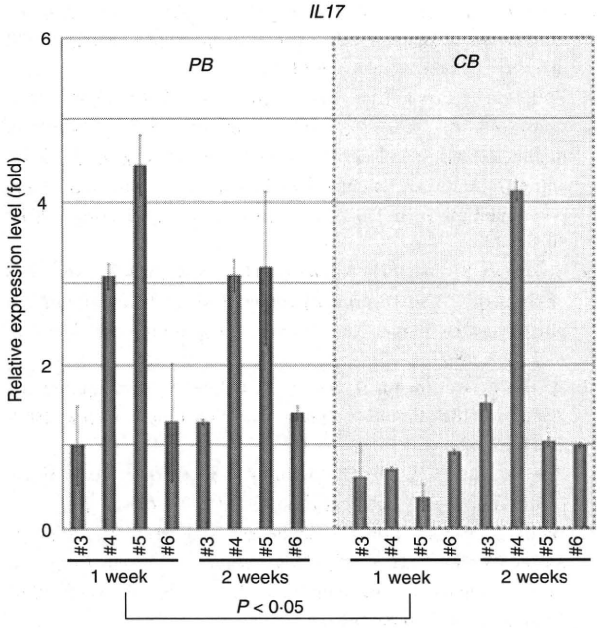

Figure 6. Quantitative polymerase chain reaction (PCR) analysis of interleukin (IL)-17 in additional samples. The expression of the *IL-17* gene in the same sample specimens as in Fig. 4 was examined and presented as in Fig 2. The data were analysed statistically and *IL-17* gene expression in peripheral blood (PB)-derived $CD4^+$ T cells was found to be significantly higher in comparison with equivalent CB-derived $CD4^+$ T cells at 1 week ($P < 0{\cdot}05$) but not at 2 weeks.

Th17 cells expand independently of T-bet or STAT-1. Ivanov *et al.*[22] have shown that the orphan nuclear receptor RORγt is the key transcription factor orchestrating the differentiation of the effector lineage. RORγt induces transcription of the gene encoding IL-17 in naïve $CD4^+$ T helper cells and is required for its expression in response to IL-6 and transforming growth factor (TGF)-β, the cytokines known to induce IL-17 expression. IL-23 is also involved in Th17 cell differentiation, but naïve T cells do not have the IL-23 receptor and are relatively refractory to IL-23 stimulation.[23,24] Although IL-23 seems to be an essential survival factor for Th17 cells, it is not required during their differentiation. It has been suggested that IL-23R expression is up-regulated on $ROR\gamma t^+$ Th17 cells in an IL-6-dependent manner. IL-23 may therefore function subsequent to IL-6/TGF-β-induced commitment to the Th17 lineage to promote cell survival and expansion and, potentially, the continued expression of IL-17 and other cytokines that characterize the Th17 phenotype. As presented in Fig. 3, the expression of the *RORγt* gene was significantly weaker in CB-derived $CD4^+$ T cells, whereas the expression of genes encoding IL-23 and the IL-23 receptor did not differ significantly between the $CD4^+$ T cells. Based on the above findings of others, it is possible that the low-level expression of the *RORγt* gene in CB-derived $CD4^+$ T cells is responsible for the absence of *IL-17* mRNA expression in those cells.

Tregs are another functional subset of T cells having anti-inflammatory properties and can cause quiescence of autoimmune diseases and prolongation of transplant function. *In vitro*, Tregs have the ability to inhibit the proliferation and production of cytokines by responder ($CD4^+$ $CD25^-$ and $CD8^+$) T cells subjected to polyclonal stimuli, as well as to down-regulate the responses of $CD8^+$ T cells, NK cells and $CD4^+$ cells to specific antigens.[25,26] These predicates translate *in vivo* to a great number of functions other than the maintenance of tolerance to self-components (prevention of autoimmune disease), such as the ability to prevent transplant rejection. Indeed, donor-specific Tregs can prevent allograft rejection in some models of murine transplant tolerance through a predominant effect on indirect alloresponses.

Foxp3 is thought to be responsible for the development of the Treg population and can act as a phenotypic marker of this fraction.[27] Tregs constitutively express CTLA-4 and there are suggestions that signalling through this pathway may be important for their function, as antibodies to CTLA-4 can inhibit Treg-mediated suppression.[28] As shown above, most of the CB-derived $CD4^+$ T cells were found to express either the *FOXP3* gene or the Foxp3 protein at higher levels compared with PB-derived $CD4^+$ T cells, suggesting that CB-derived $CD4^+$ T cells frequently include a potent Treg population.

As described above, *IL-17* mRNA was more detectable in PB-derived $CD4^+$ cells while *FOXP3* mRNA expression was higher in CB-derived $CD4^+$ cells. Post-transcriptional regulation, as well as differences in mRNA and protein turnover rates, can cause discrepancies between mRNA and protein expression and thus the differences observed in the mRNA expression do not necessary directly indicate those in protein expression.[29] Indeed, we observed some discrepancy between the levels of mRNA and protein with regard to Foxp3 expression in CB-derived $CD4^+$ T cells, as presented above. Nevertheless, changes in mRNA expression are mediated by the alteration of transcriptional regulation, and thus should indicate the differentiation ability of the cells. Therefore, our data indicate that CB-derived $CD4^+$ T cells tend frequently to include potent Tregs, while PB-derived $CD4^+$ T cells tend to include potent IL-17-secreting cells. As described above, DLI with donor CB-derived activated $CD4^+$ T cells is currently becoming established as a routine therapeutic strategy in Japan. It has been proposed that the skewing of responses towards Th17 or Th1 cells and away from Tregs may be responsible for the development and/or progression of autoimmune diseases or acute transplant rejection, and it may thus also be speculated that CB-derived $CD4^+$ T cells are more appropriate for DLI than PB-derived $CD4^+$ T cells.

However, our data also indicate the presence of individual, donor-dependent variations in the characteristics of activated $CD4^+$ T cells derived from CB and PB. More-

over, activated $CD4^+$ T cells do not consist of a single population and should include several distinct functional subsets of $CD4^+$ T cells. Therefore, it is important to clarify the characteristics of activated $CD4^+$ T cells in each preparation to predict the therapeutic effect of DLI in each clinical case.

In summary, our findings demonstrate a difference in gene expression between activated $CD4^+$ T cells derived from CB and those derived from PB. The higher level of *FOXP3* gene expression and the lower level of *IL-17* gene expression in CB-derived $CD4^+$ T cells may indicate that these cells have potential as immunomodulators in DLI therapy. Further detailed analysis should reveal the advantages of activated $CD4^+$ T cells from CB in DLI.

Acknowledgements

We thank the Tokyo Cord Blood Bank for the distribution of cord blood for research use. This work was supported by a grant from the Japan Health Sciences Foundation for Research on Publicly Essential Drugs and Medical Devices (KHC2032), Health and Labour Sciences Research Grants (the 3rd term comprehensive 10-year strategy for cancer control H19-010, Research on Children and Families H18-005, Research on Human Genome Tailor-made and Research on Publicly Essential Drugs and Medical Devices H18-005), and a Grant for Child Health and Development from the Ministry of Health, Labour and Welfare of Japan. It was also supported by CREST, JST.

Disclosures

No competing personal or financial interests exist for any of the authors in relation to this manuscript.

References

1 Loren AW, Porter DL. Donor leukocyte infusions after unrelated donor hematopoietic stem cell transplantation. *Curr Opin Oncol* 2006; **18**:107–14.
2 Roush KS, Hillyer CD. Donor lymphocyte infusion therapy. *Transfus Med Rev* 2002; **16**:161–76.
3 Alyea EP, Soiffer RJ, Canning C *et al.* Toxicity and efficacy of defined doses of CD4(+) donor lymphocytes for treatment of relapse after allogeneic bone marrow transplant. *Blood* 1998; **91**:3671–80.
4 Giralt S, Hester J, Huh Y *et al.* CD8-depleted donor lymphocyte infusion as treatment for relapsed chronic myelogenous leukemia after allogeneic bone marrow transplantation. *Blood* 1995; **86**:4337–43.
5 Tomizawa D, Aoki Y, Nagasawa M *et al.* Novel adopted immunotherapy for mixed chimerism after unrelated cord blood transplantation in Omenn syndrome. *Eur J Haematol* 2005; **75**:441–4.
6 Cohena Y, Nagler A. Hematopoietic stem-cell transplantation using umbilical-cord blood. *Leuk Lymphoma* 2003; **44**:1287–99.
7 Parmar S, Robinson SN, Komanduri K *et al.* Ex vivo expanded umbilical cord blood T cells maintain naive phenotype and TCR diversity. *Cytotherapy* 2006; **8**:149–57.
8 Robinson KL, Ayello J, Hughes R, van de Ven C, Issitt L, Kurtzberg J, Cairo MS. Ex vivo expansion, maturation, and activation of umbilical cord blood-derived T lymphocytes with IL-2, IL-12, anti-CD3, and IL-7. Potential for adoptive cellular immunotherapy post-umbilical cord blood transplantation. *Exp Hematol* 2002; **30**:245–51.
9 Miyagawa Y, Okita H, Nakaijima H *et al.* Inducible expression of chimeric EWS/ETS proteins confers Ewing's family tumor-like phenotypes to human mesenchymal progenitor cells. *Mol Cell Biol* 2008; **28**:2125–37.
10 Werlen G, Hausmann B, Naeher D, Palmer E. Signaling life and death in the thymus: timing is everything. *Science* 2003; **299**:1859–63.
11 Riley JL, June CH. The CD28 family: a T-cell rheostat for therapeutic control of T-cell activation. *Blood* 2005; **105**:13–21.
12 Woo EY, Yeh H, Chu CS, Schlienger K, Carroll RG, Riley JL, Kaiser LR, June CH. Cutting edge: regulatory T cells from lung cancer patients directly inhibit autologous T cell proliferation. *J Immunol* 2002; **168**:4272–6.
13 Azuma H, Yamada Y, Shibuya-Fujiwara N *et al.* Functional evaluation of ex vivo expanded cord blood lymphocytes: possible use for adoptive cellular immunotherapy. *Exp Hematol* 2002; **30**:346–51.
14 Afzali B, Lombardi G, Lechler RI, Lord GM. The role of T helper 17 (Th17) and regulatory T cells (Treg) in human organ transplantation and autoimmune disease. *Clin Exp Immunol* 2007; **148**:32–46.
15 Castellino F, Germain RN. Cooperation between CD4+ and CD8+ T cells: when, where, and how. *Annu Rev Immunol* 2006; **24**:519–40.
16 Reiner SL. Development in motion: helper T cells at work. *Cell* 2007; **129**:33–6.
17 Bi Y, Liu G, Yang R. Th17 cell induction and immune regulatory effects. *J Cell Physiol* 2007; **211**:273–8.
18 Fossiez F, Djossou O, Chomarat P *et al.* T cell interleukin-17 induces stromal cells to produce proinflammatory and hematopoietic cytokines. *J Exp Med* 1996; **183**:2593–603.
19 Loong CC, Hsieh HG, Lui WY, Chen A, Lin CY. Evidence for the early involvement of interleukin 17 in human and experimental renal allograft rejection. *J Pathol* 2002; **197**:322–32.
20 Van Kooten C, Boonstra JG, Paape ME *et al.* Interleukin-17 activates human renal epithelial cells in vitro and is expressed during renal allograft rejection. *J Am Soc Nephrol* 1998; **9**:1526–34.
21 Vanaudenaerde BM, Dupont LJ, Wuyts WA *et al.* The role of interleukin-17 during acute rejection after lung transplantation. *Eur Respir J* 2006; **27**:779–87.
22 Ivanov II, McKenzie BS, Zhou L, Tadokoro CE, Lepelley A, Lafaille JJ, Cua DJ, Littman DR. The orphan nuclear receptor RORgammat directs the differentiation program of proinflammatory IL-17+ T helper cells. *Cell* 2006; **126**:1121–33.
23 Langrish CL, Chen Y, Blumenschein WM *et al.* IL-23 drives a pathogenic T cell population that induces autoimmune inflammation. *J Exp Med* 2005; **201**:233–40.
24 Oppmann B, Lesley R, Blom B *et al.* Novel p19 protein engages IL-12p40 to form a cytokine, IL-23, with biological activities similar as well as distinct from IL-12. *Immunity* 2000; **13**: 715–25.

25 Dieckmann D, Plottner H, Berchtold S, Berger T, Schuler G. Ex vivo isolation and characterization of CD4(+) CD25(+) T cells with regulatory properties from human blood. *J Exp Med* 2001; **193**:1303–10.

26 Wing K, Lindgren S, Kollberg G, Lundgren A, Harris RA, Rudin A, Lundin S, Suri-Payer E. CD4 T cell activation by myelin oligodendrocyte glycoprotein is suppressed by adult but not cord blood CD25+ T cells. *Eur J Immunol* 2003; **33**:579–87.

27 Wan YY, Flavell RA. Identifying Foxp3-expressing suppressor T cells with a bicistronic reporter. *Pro Natl Acad Sci USA* 2005; **102**:5126–31.

28 Read S, Greenwald R, Izcue A, Robinson N, Mandelbrot D, Francisco L, Sharpe AH, Powrie F. Blockade of CTLA-4 on CD4+ CD25+ regulatory T cells abrogates their function in vivo. *J Immunol* 2006; **177**:4376–83.

29 Hack CJ. Integrated transcriptome and proteome data: the challenges ahead. *Brief Funct Genomic Proteomic* 2004; **3**:212–9.

The endothelial antigen ESAM marks primitive hematopoietic progenitors throughout life in mice

Takafumi Yokota,[1] Kenji Oritani,[1] Stefan Butz,[2] Koichi Kokame,[3] Paul W. Kincade,[4] Toshiyuki Miyata,[3] Dietmar Vestweber,[2] and Yuzuru Kanakura[1]

[1]Department of Hematology and Oncology, Osaka University Graduate School of Medicine, Suita, Japan; [2]Department of Vascular Cell Biology, Max-Planck-Institute for Molecular Biomedicine, Münster, Germany; [3]National Cardiovascular Center Research Institute, Osaka, Japan; and [4]Immunobiology and Cancer Program, Oklahoma Medical Research Foundation, Oklahoma City

Although recent advances have enabled hematopoietic stem cells (HSCs) to be enriched to near purity, more information about their characteristics will improve our understanding of their development and stage-related functions. Here, using microarray technology, we identified endothelial cell-selective adhesion molecule (ESAM) as a novel marker for murine HSCs in fetal liver. *Esam* was expressed at high levels within a Rag1$^-$ c-kit^{Hi} Sca1$^+$ HSC-enriched fraction, but sharply down-regulated with activation of the Rag1 locus, a valid marker for the most primitive lymphoid progenitors in E14.5 liver. The HSC-enriched fraction could be subdivided into 2 on the basis of ESAM levels. Among endothelial antigens on hematopoietic progenitors, ESAM expression showed intimate correlation with HSC activity. The ESAM^{Hi} population was highly enriched for multipotent myeloid-erythroid progenitors and primitive progenitors with lymphopoietic activity, and exclusively reconstituted long-term lymphohematopoiesis in lethally irradiated recipients. Tie2$^+$ c-kit$^+$ lymphohematopoietic cells in the E9.5–10.5 aorta-gonad-mesonephros region also expressed high levels of ESAM. Furthermore, ESAM was detected on primitive hematopoietic progenitors in adult bone marrow. Interestingly, ESAM expression in the HSC-enriched fraction was up-regulated in aged mice. We conclude that ESAM marks HSC in murine fetal liver and will facilitate studies of hematopoiesis throughout life. (Blood. 2009;113:2914-2923)

Introduction

Hematopoietic stem cells (HSCs) are defined as cells with the capacity for self-renewal as well as differentiation into multilineage blood cells, maintaining the immune system throughout life. A large body of information exists about molecular mechanisms involved in maintaining their integrity, and many studies have attempted to identify unique markers associated with these extremely rare cells. In bone marrow of adult mice, the Lin$^-$ c-kit^{Hi} Sca1$^+$ CD34$^{-/Lo}$ Thy1.1^{Lo} subset is known to include HSCs with long-term repopulating capacity.[1] However, several of these parameters differ between strains of mice, change dramatically during developmental age or inflammation, and are expressed on many non-HSCs.[2-4] The recent identification of CD150/SLAM as stable markers made it possible to increase the purity of HSCs even in aged mice or cyclophosphamide/granulocyte colony-stimulating factor-treated mice with mobilized progenitors.[5] However, even the most highly purified HSCs are heterogeneous, and it may eventually be possible to associate discrete functions or activity states with subpopulations. Additional authentic HSC markers could have utility in attempts to rescue hematopoietic disorders using hematopoietic progenitors obtained from reprogrammed adult tissues.[6,7]

HSCs are thought to arise initially from hemogenic endothelium, which can produce hematopoietic cells as well as endothelial cells. Therefore, it is not surprising that HSCs share some endothelial properties at early developmental stages.[8,9] For example, the CD34 sialomucin and Tie2, an angiopoietin receptor, are expressed on HSCs in E10–11 embryos.[10,11] Endoglin and vascular-endothelial cadherin are additional endothelial markers found on fetal HSCs.[8,12] However, the expression of many of these antigens declines on HSCs at later stages of development.[3,4,13] It is interesting that the expression of CD34 is restored when adult HSCs are driven into cycle by 5-fluorouracil or granulocyte colony-stimulating factor administration.[14,15] CD11b/Mac-1 is an adhesion molecule that is similarly dependent on developmental age and activation status.[16] In contrast to these patterns, endomucin is a CD34-like sialomucin that marks HSCs from E10 and throughout subsequent development.[17] Each of these advances offered the promise of learning more about how HSCs arise de novo and function throughout life.

We previously determined that the most primitive cells with lymphopoietic potential first develop in the para-aortic splanchnopleura (PSp)/aorta-gonad-mesonephros (AGM) region of embryos, and we tracked expression of the *Rag1* lymphoid gene.[18,19] To extend those findings, we searched for genes that might be differentially expressed at the very earliest stages of lymphopoiesis. We here show that endothelial cell-selective adhesion molecule (ESAM) is a durable and effective marker of HSCs. Indeed, ESAM was expressed throughout life and could be used as a gating parameter for sorting long-term repopulating HSCs.

Methods

Animals

Rag1/GFP knockin mice (CD45.2 alloantigen) were described.[20,21] Mice of the corresponding wild-type (WT) C57BL/6 were obtained from Japan Clea (Shizuoka, Japan). Mating homozygous male Rag1/GFP knockin mice with WT C57BL/6 female mice generated heterozygous Rag1/GFP knockin

Submitted July 4, 2008; accepted November 1, 2008. Prepublished online as *Blood* First Edition paper, December 18, 2008; DOI 10.1182/blood-2008-07-167106.

An Inside *Blood* analysis of this article appears at the front of this issue.

The online version of this article contains a data supplement.

The publication costs of this article were defrayed in part by page charge payment. Therefore, and solely to indicate this fact, this article is hereby marked "advertisement" in accordance with 18 USC section 1734.

fetuses. The day of vaginal plug observation was considered as day 0.5 postcoitum (E0.5). In some experiments, we purchased pregnant C57BL/6 mice from Japan Clea and used their fetuses. The congenic C57BL/6 strain (C57BL/6SJL; CD45.1 alloantigen) was purchased from The Jackson Laboratory (Bar Harbor, ME) and used in transplantation experiments. The experimental designs of this study were approved by the committee of Osaka University for animal studies.

Antibodies

Phycoerythrin (PE)–conjugated anti-Sca1 (Ly6A/E; D7), CD48 (HM48-1), CD11b/Mac-1 (M1/70), Gr-1 (RB6-8C5), CD19 (1D3), CD4 (L3T4), and CD8a (53-6.7) monoclonal antibodies (mAbs), biotinylated anti-CD45.2(104) mAb, allophycocyanin (APC)–conjugated anti-CD11b/Mac-1 (M1/70) and c-kit (2B8) mAbs, and PE-Texas red tandem-conjugated (PE-TR) streptavidin were purchased from BD Biosciences PharMingen (San Diego, CA). PE-conjugated anti-CD34 (RAM34), CD31/PECAM-1(390), CD105/Endoglin (MJ7/18), and Tie2 (TEK4) mAbs, PE-Cy7–conjugated anti-Sca1 (Ly6A/E; D7) mAb, and APC-conjugated anti CD45.1 (A20) mAbs were purchased from eBioscience (San Diego, CA). A rat anti–mouse ESAM mAb (1G8), a rabbit anti–mouse ESAM polyclonal Ab (VE19), and a rabbit preimmune IgG were prepared in our hands.[22] A fluorescein isothiocyanate (FITC)–conjugated goat anti–rat IgG (H+L) Ab purchased from Southern Biotechnology (Birmingham, AL), a PE-conjugated goat antirat Ig Ab purchased from BD Biosciences PharMingen, or AlexaFluor 488 goat anti–rabbit IgG (H+L) Ab purchased from Invitrogen (Carlsbad, CA) was used as a second Ab for the anti-ESAM Abs. A PE-conjugated hamster IgG1 was purchased from BD Biosciences PharMingen and used as a control for a PE-conjugated anti-CD48. FITC-conjugated anti-CD11b/Mac-1 (M1/70), Gr-1 (RB6–8C5), TER-119, CD45R/B220 (RA3-6B2), and CD3e (145-2C11) were purchased from BD Biosciences PharMingen and used as lineage markers in adult studies.

Cell sorting

Fetal liver or cells obtained from adult femurs and tibias of heterozygous Rag1/GFP knockin mice were harvested and subjected to cell sorting as previously described.[18] In the first step, Rag1$^-$ or Rag1^{Lo} cells were sorted according to levels of green fluorescent protein (GFP) expression. Background auto-fluorescence was discriminated from authentic GFP by collecting data in 2 fluorescence channels without compensation. Under these conditions, even extremely low levels of fluorescence specific to GFP knockin mice were obvious on 2-color diagonal plots. The purity of the sorted cells in the first step was more than 95%. The sorted cells were incubated with anti-FcR (2.4G2) before staining with PE-anti-Sca1 and APC-anti-c-kit antibodies, suspended in 7-amino-actinomycin D (7-AAD)–containing buffer, and subjected to a second round of sorting. Dead cells stained with 7-AAD and a few contaminating cells with inappropriate GFP levels were gated out, and the cells were then fractionated according to Sca1 and c-kit to obtain Rag1$^-$ c-kit^{Hi} Sca1$^+$ HSCs and Rag1^{Lo} ckit^{Hi} Sca1$^+$, early lymphoid progenitors (ELPs). The cell sorting was performed with FACSaria using the FACSDiva program (BD Biosciences, San Jose, CA). The sorting gates used to isolate HSCs and ELPs from E14.5 fetal liver for gene array experiments ("Gene arrays") are shown in Figure S1 (available on the *Blood* website; see the Supplemental Materials link at the top of the online article).

In the sorting experiments with ESAM expression, Rag1/GFP$^-$ cells were first sorted from fetal tissues or adult bone marrow. Then the cells were stained with rat anti–mouse ESAM mAb (1G8) followed by FITC-goat anti–rat IgG or PE-goat anti–rat Ig, respectively. After the staining for ESAM, E14.5 fetal liver Rag1/GFP$^-$ cells were stained with PE–anti-Sca1 and APC-anti–c-kit antibodies. For PSp/AGM or yolk sac (YS) cells of E9.5-10.5 embryos, a PE-anti–Tie2 Ab was used instead of a PE-anti–Sca1 Ab. The adult marrow Rag1/GFP$^-$ cells were stained with FITC-anti-Lin (Mac-1, Gr-1, TER119, CD45R/B220, CD3e), PE-Cy7–anti-Sca1, and APC-anti–c-kit Abs. Then the cells were suspended in 7-AAD–containing buffer and subjected to a second round of sorting.

Gene arrays

Total RNAs were isolated from the Rag1$^-$ ckit^{Hi} Sca1$^+$, HSC-enriched fraction and the Rag1^{Lo} ckit^{Hi} Sca1$^+$, ELP-enriched fraction, both of which were isolated from mouse E14.5 fetal liver. From the aliquot of each RNA (24 ng), biotin-labeled cRNA was prepared using GeneChip 2-Cycle Target Labeling and Control Reagents (Affymetrix, Santa Clara, CA) according to the manual. The cRNA was fragmented and hybridized to Mouse Genome 430 2.0 Array (Affymetrix) using a GeneChip Hybridization, Wash, and Stain Kit (Affymetrix). Fluorescent signals were scanned by GeneChip Scanner 3000, and the data were analyzed by GeneSpring GX software (Agilent Technologies, Palo Alto, CA). *Bacillus subtilis* genes on the arrays were used as negative controls for background subtraction. All values of the genes in each array were divided by the value of glyceraldehyde-3-phosphate dehydrogenase (*Gapdh*) gene. The Cross-Gene Error Model was used to estimate measurement precision by combining variability of gene expression data. The experiments were duplicated to confirm reproducibility of the data. All microarray data have been deposited with CIBEX, National Institute of Genetics DDBJ (DNA Data Bank of Japan) under the accession number CBX73.

Flow cytometry

Rag1/GFP$^-$ cells of E14.5 fetal liver were incubated with rat anti–mouse ESAM mAb (1G8) followed by FITC-goat anti–rat IgG. Then the cells were incubated with a rat anti–mouse FcRII/III (2.4G2) and subsequently stained with PE-Cy7–anti-Sca1 and APC-anti–c-kit in combination with PE-anti–CD34, CD31/PECAM1, CD105/Endoglin, or Tie2 mAbs. The cells were suspended in 7-AAD–containing buffer and subjected to flow cytometry analyses, performed with FACSaria using the FACSDiva program (BD Biosciences).

In the other experiments, cultured cells or recovered cells from transplanted mice were incubated with anti-FcR and then stained with PE-, APC-conjugated mAbs and/or a biotinylated Ab followed by PE-TR-streptavidin as indicated in each figure. The flow cytometry analyses were performed with FACScalibur using the Cellquest program (BD Biosciences). The data analyses were done with FlowJo software (TreeStar, Ashland, OR).

Methylcellulose culture

A total of 500 or 100 cells of each sorted fraction (Rag1/GFP$^-$ ckit^{Hi} Sca1$^+$ ESAM1$^{-/Lo}$ or Rag1/GFP$^-$ ckit^{Hi} Sca1$^+$ ESAM1^{Hi} of fetal liver or adult marrow, respectively) were cultured in Iscove modified Dulbecco medium-based methylcellulose medium supplemented with 50 ng/mL of recombinant mouse (rm) stem cell factor (SCF), 10 ng/mL of rm interleukin-3 (IL-3), 10 ng/mL of recombinant human IL-6, and 3 U/mL of recombinant human erythropoietin (Methocult GF 3434; StemCell Technologies, Vancouver, BC). After 8 to 10 days, colonies were enumerated and classified as granulocyte colony-forming units (CFU-G); macrophage colony-forming units (CFU-M); granulocyte-macrophage colony-forming units (CFU-GM); erythroid burst-forming units (BFU-E); or mixed erythroid-myeloid colony-forming units (CFU-Mix) according to shape and color under an inverted microscope. In some experiments, colony types were morphologically certified by examination of cytospin preparations after May-Grünwald/Giemsa staining.

Stromal coculture and limiting dilution assays

The murine bone marrow stromal cell line MS-5 was generously provided by Dr J. Mori (Niigata University, Niigata, Japan). Nonirradiated MS-5 stromal cells were prepared at a concentration of 5×10^4 cells/well in 24-well tissue plates 1 day before the seeding of sorted cells at a concentration of 50 cells/mL. Cells were cultured in α-minimum essential medium (Invitrogen) supplemented with 10% fetal calf serum (FCS), rm SCF (10 ng/mL), rm Flt3-ligand (20 ng/mL), and rm IL-7 (1 ng/mL). The cultures were fed every 4 days by removing half of the medium and replacing it with fresh medium, and maintained for 6 or 10 days. Cytokines were freshly added with each feeding.

The frequencies of lymphohematopoietic progenitors in the fetal liver–derived Rag1/GFP$^-$ ckit^{Hi} Sca1$^+$ ESAM$^{-/Lo}$ or Rag1/GFP$^-$ ckit^{Hi} Sca1$^+$ ESAM^{Hi} fraction were determined by plating the sorted cells in limiting dilution assays using 96-well flat bottom plates. Pre-established MS-5 stromal cell layers were plated with 1, 2, 4, 8, or 50 cells each using the Automated Cell Deposition Unit of the FACSaria (BD Biosciences). Cells were cultured in α-minimum essential medium supplemented with 10% FCS, rm SCF (10 ng/mL), rm Flt3-ligand (20 ng/mL), and rm IL-7 (1 ng/mL). At 10 days of culture, wells were inspected for the presence of hematopoietic clones. Positive wells were harvested, stained, and analyzed by flow cytometry for the presence of CD19$^+$ Gr-1$^-$ B lineage cells. The frequencies of progenitors were calculated by linear regression analysis on the basis of Poisson distribution as the reciprocal of the concentration of test cells that gave 37% negative cultures.

Competitive repopulation assay

The Ly5 system was adapted to a competitive repopulation assay. A total of 1000 Rag1/GFP$^-$ c-kit^{Hi} Sca1$^+$ ESAM$^{-/Lo}$ or Rag1/GFP$^-$ c-kit^{Hi} Sca1$^+$ ESAM^{Hi} cells sorted from fetal liver of E14.5 Rag1/GFP heterozygous embryos (CD45.2) were mixed with 2×10^5 unfractionated adult bone marrow cells obtained from WT C57BL/6-Ly5.1 (CD45.1) mice and were transplanted into C57BL/6-Ly5.1 mice irradiated at a dose of 10 Gy. At 5 weeks after transplantation, peripheral blood cells of the recipients were colleted by retro-orbital bleeding and were stained with APC-conjugated anti-CD45.1 and biotinylated anti-CD45.2 Abs followed by PE-TR streptavidin. The cells were simultaneously stained with PE-conjugated anti–Mac-1 and Gr-1 Abs, or PE-conjugated anti-CD19 Ab, or PE-conjugated anti-CD4 and CD8a Abs. Twenty weeks after transplantation, all recipients were killed, and reconstitution of CD45.2$^+$ myeloid, B, or T cells was confirmed by flow cytometry in the bone marrow, spleen, and thymus, respectively. For the second transplantation, bone marrow cells of primary recipients with CD45.2 engraftment were transferred into 10 Gy-irradiated C57BL/6-Ly5.1 mice (10^6 whole bone marrow cells per recipient). After 20 weeks, contribution of CD45.2 cells to the hematopoietic reconstitution was evaluated in the second recipients.

Cell preparation from PSp/AGM and YS

To examine the phenotype or function of hematopoietic progenitors in the PSp/AGM and the YS of early embryos, cells were prepared as previously described.[19] Briefly, tissues were dissociated by incubation with dispase II (Roche Diagnostics, Mannheim, Germany) for 20 minutes at 37°C and cell dissociation buffer (Invitrogen) for 20 minutes at 37°C followed by vigorous pipetting. The cells were then suspended in phosphate-buffered saline containing 3% FCS and stained with the Abs indicated in each experiment.

Statistical methods

Statistical analysis was carried out by standard Student *t* tests. Error bars used throughout indicate SD of the mean.

Results

Identification of ESAM as a marker of primitive hematopoietic cells

Microarrays were performed as part of an effort to characterize the initial transition of fetal HSCs to primitive lymphopoietic cells. The comparisons involved mRNA from Rag1^{Lo} ckit^{Hi} Sca1$^+$, ELPs, and the HSC-enriched Rag1$^-$ ckit^{Hi} Sca1$^+$ fraction isolated from E14.5 fetal liver (Figure S1).

Consistent with previous analyses,[12,23,24] *Evi1*, *CD41*, and *Endoglin* were highly expressed by fetal HSCs (Figure 1). *Esam* transcripts were conspicuous in the HSC fraction and attracted attention because of a sharp down-regulation on differentiation to ELP (Figure 1). Real-time PCR using *Esam* specific primers verified the results of these microarrays (data not shown).

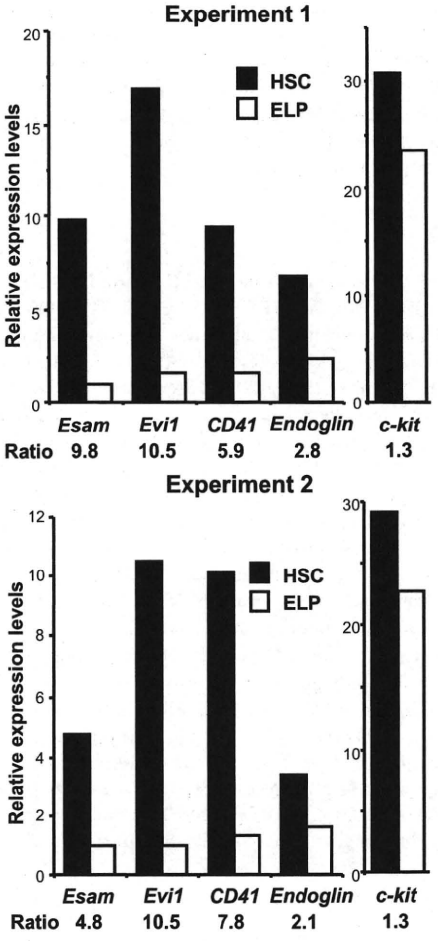

Figure 1. *Esam* gene is preferentially expressed in the HSC fraction of E14.5 fetal liver. Microarray analyses comparing HSC-enriched and ELP-enriched populations were performed. Two independent tests depicted the *Esam* gene as preferentially expressed in the HSC-enriched population. Results are shown as relative expression levels of each gene comparing with that of *Gapdh* of which value is 100. Ratio was calculated by [HSC level]/[ELP level] in each gene. The relative expression levels of *c-kit* were also shown as internal quality controls.

ESAM can be used to subdivide hematopoietic progenitors in fetal liver

The availability of a rat antimouse ESAM mAb (clone 1G8) facilitated characterization of mononuclear cells obtained from E14.5 fetal liver. A majority of ESAM$^+$ cells were found in the c-kit^{Hi} fraction (Figure 2A left). ESAM expression also correlated with Sca1 (Figure 2A middle). These observations suggested that ESAM might substitute for at least one of the 2 most widely used HSC markers. Indeed, cells in the Sca1^{Hi} ESAM^{Hi} gate were almost homogeneous with respect to high c-kit expression (Figure 2A right).

The c-kit^{Hi} Sca1$^+$ fraction, known to include all conventional HSCs, was divided into 2 categories according to ESAM staining (Figure 2B left and middle). The subpopulation with the highest density of ESAM was enriched for c-kit^{Hi} Sca1^{Hi} cells, whereas ones with negative or low levels of ESAM were found in the c-kit^{Hi} Sca1^{Lo} subset (Figure 2B right). The latter are thought to be enriched with respect to committed myelo-erythroid progenitors.[25] Similar results were obtained with a rabbit antimouse ESAM polyclonal Ab (VE19) (data not shown).

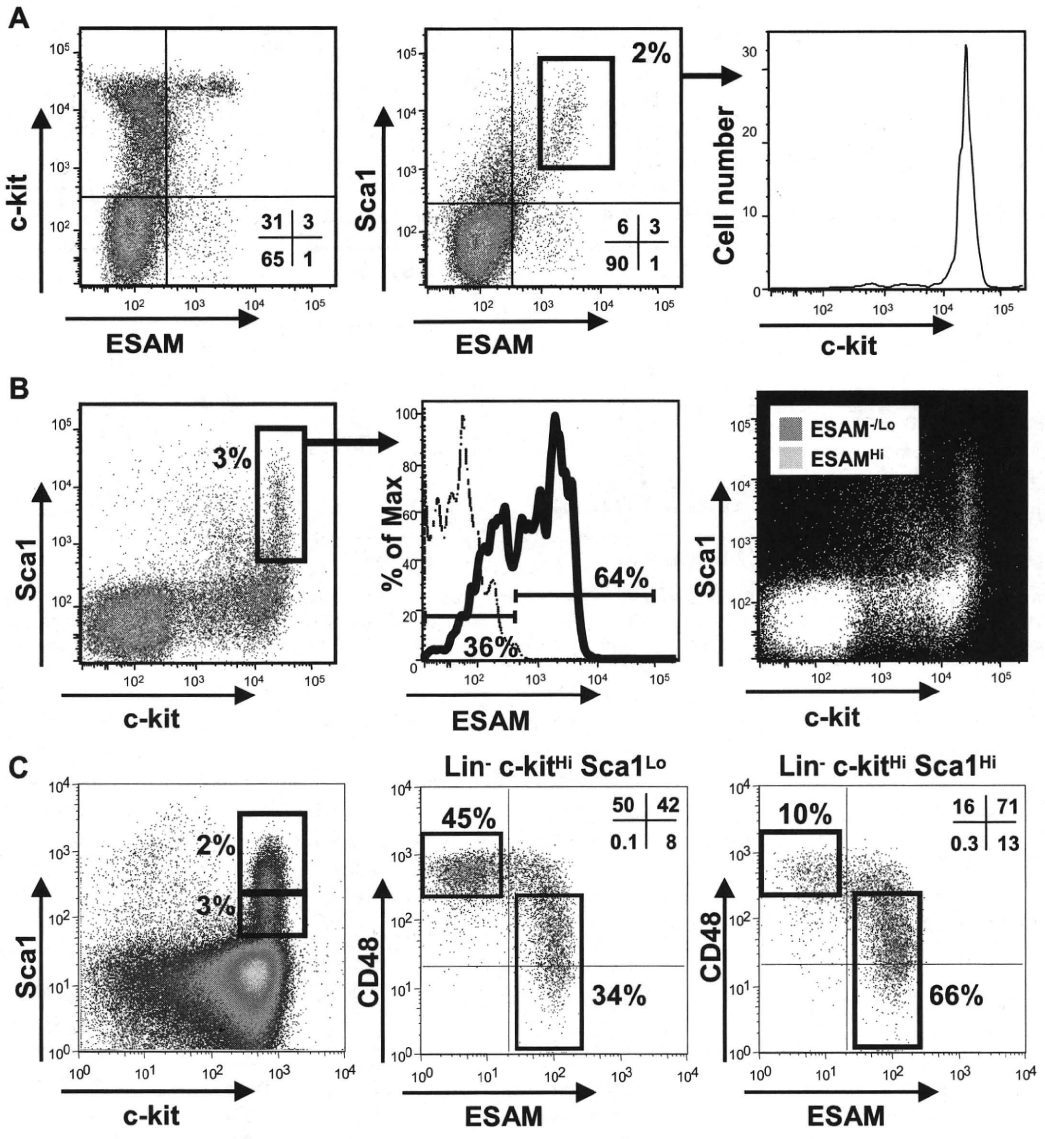

Figure 2. Specific expression of ESAM on HSC-enriched fraction of E14.5 fetal liver. Flow cytometric analysis was performed for Rag1/GFP$^-$ cells of E14.5 fetal liver using anti-c-kit, anti-Sca1, and anti-ESAM Abs. First, Rag1/GFP$^-$ cells were sorted from E14.5 fetal liver of Rag1/GFP knockin heterozygous fetuses with high purity. The sorted cells were incubated with a purified rat anti–mouse ESAM Ab (1G8) followed by goat anti–rat IgG-FITC. The cells were then stained with anti-c-kit-APC, anti-Sca1-PE, and 7-AAD. To minimize the nonspecific binding of anti-c-kit and Sca1 mAbs to the cells wearing goat anti–rat IgG-FITC, the cells were incubated with a rat anti–mouse FcRII/III Ab before the anti-c-kit and Sca1 staining. (A) The Rag1/GFP$^-$ cells were analyzed with respect to expression of ESAM, c-kit, and Sca1 (Left, middle). Expression of c-kit in the Sca1^{Hi} ESAM^{Hi} cells (middle, inset) is presented (right). (B) The conventional c-kit^{Hi} Sca1$^+$ fraction (left, inset) could be divided into 2 fractions, ESAM$^{-/Lo}$ and ESAM^{Hi} (middle). The cells were stained with an isotype control IgG (dashed line) or with the anti-ESAM Ab (solid line). The ESAM^{Hi} cells (yellow) were found as c-kit^{Hi} Sca1^{Hi}, whereas the ESAM$^{-/Lo}$ cells (pink) were c-kit^{Hi} Sca1^{Lo} (right). (C) Six-color flow cytometric analysis using an anti-ESAM Ab followed by goat anti–rat IgG-FITC, a PE-anti-CD48 Ab, biotin-anti-lineage marker Abs (TER119, Gr1, CD3, CD45R/B220) followed by SA-PETR, a PE-Cy7-anti-Sca1 Ab, an APC-anti-c-kit, and 7-AAD was performed for E14.5 fetal liver cells of WT C57B6 embryos. The profile of Lin$^-$ cells regarding c-kit and Sca1 expression is shown in the left. The Lin$^-$ c-kit^{Hi} Sca1^{Lo} and Lin$^-$ c-kit^{Hi} Sca1^{Hi} fractions gated in the left panel were analyzed with respect to expression of ESAM and CD48 (middle and right). The percentage of cells in each gate is indicated in each panel.

When E14.5 fetal liver cells of WT C57B6 mice and traditional markers of fetal liver HSCs were used instead of the Rag1/GFP knockin mice, essentially identical results were obtained (Figure 2C). This analysis was performed with CD48 expression, one of the SLAM family members recently shown to conversely relate with HSC activity in fetal liver.[26] Lin$^-$ c-kit^{Hi} Sca1$^+$ cells could be divided into ESAM$^-$ and ESAM$^+$ fractions, and a subpopulation with higher Sca1 expression was more enriched with ESAM$^+$ cells (Figure 2C middle and right). CD48 expression tended to increase along with down-regulation of ESAM. Indeed, the Lin$^-$ c-kit^{Hi} Sca1$^+$ fraction was found to consist of 2 major subpopulations, CD48^{Hi} ESAM$^-$ and CD48$^{-/Lo}$ ESAM$^+$. Thus, ESAM is conspicuously expressed on immature hematopoietic cells in fetal liver and seems to conversely relate to lineage progression.

ESAM expression is closely associated with fetal HSCs among endothelial markers

Next we evaluated how ESAM corresponds to other endothelial antigens that were previously identified on fetal hematopoietic progenitors. CD34 and CD31/PECAM1 were uniformly present on Rag1$^-$ c-kit^{Hi} Sca1$^+$ cells in E14.5 fetal liver (Figure 3A,B). Neither could resolve the Rag1$^-$ c-kit^{Hi} Sca1$^+$ cells into ESAM^{Hi} and ESAM$^{-/Lo}$ fractions, and even showed a slightly inverse relationship with ESAM expression on early progenitors. Expression profiles of Endoglin and

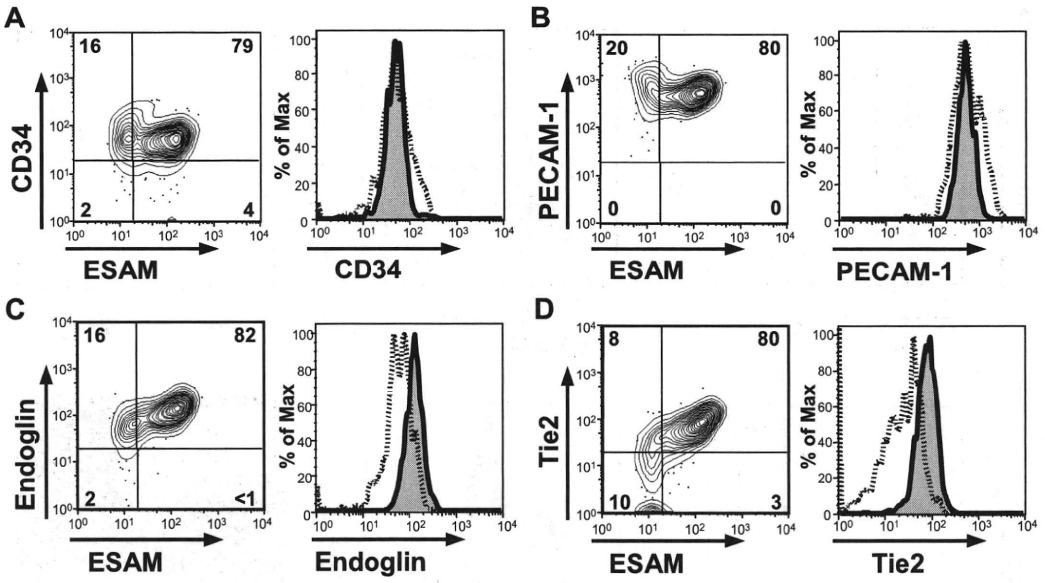

Figure 3. Expression of ESAM and other endothelial antigens on fetal liver HSC fraction. The expression pattern of ESAM on Rag1/GFP$^-$ c-kit^{Hi} Sca1$^+$ cells of E14.5 fetal liver was compared with other endothelial cell-related antigens, CD34 (A), CD31/PECAM1 (B), Endoglin (C), and Tie2 (D). The percentage of cells in subpopulation is shown. In the histograms, the staining patterns of ESAM$^{-/Lo}$ cells are indicated with dashed lines; those of ESAM^{Hi} cells are tinted and indicated with solid lines.

Tie2 did correlate with ESAM (Figure 3C,D). However, although the primitive ESAM^{Hi} fraction uniformly expressed high levels of Endoglin and Tie2, many of the more differentiated ESAM$^{-/Lo}$ cells still retained the 2 markers. These results suggest that ESAM might be a more useful marker of HSCs than other endothelial antigens and could represent an important tool for fetal stem cell studies.

ESAM is useful to enrich primitive multipotent progenitors from fetal liver

To evaluate whether ESAM expression can enrich primitive progenitors in fetuses, we compared the clonogenic potential in methylcellulose cultures of the ESAM$^{-/Lo}$ and ESAM^{Hi} cells in the Rag1$^-$ ckit^{Hi} Sca1$^+$ HSC fraction of E14.5 fetal liver. Cells in the ESAM^{Hi} fraction formed more colonies with larger size than those in the ESAM$^{-/Lo}$ fraction (Figure 4). In particular, most CFU-Mix, primitive progenitors with both myeloid and erythroid potential, were found in the ESAM^{Hi} fraction (Figure 4A).

Next we analyzed the lymphopoietic potential of cells resolved on the basis of ESAM in cocultures with the MS5 bone marrow stromal cell line. The culture media contained SCF, Flt3-ligand, and IL-7, factors that effectively generate CD19$^+$ B lymphoid cells as well as Mac1$^+$ myeloid cells.[18] When 500 cells were cultured in individual wells of 6-well plates, both ESAM$^{-/Lo}$ and ESAM^{Hi} fractions produced CD19$^+$ cells and Mac1$^+$ cells (Figure 5A). However, we observed that most of the hematopoietic colonies from ESAM^{Hi} cells grew beneath the MS5 stromal cell layer, although this was not the case with ESAM$^{-/Lo}$ cells (data not shown). Moreover, the lymphohematopoietic cells from ESAM^{Hi} cells continued to expand explosively after 6 days of coculture and gave rise to approximately 50 000 cells per input progenitor by day 10 (Figure 5B).

Authentic HSCs are characterized as having both lymphoid and myeloid potential.[8,27] To compare numbers of primitive lymphohematopoietic progenitors in the ESAM^{Hi} and ESAM$^{-/Lo}$ fractions, we performed in vitro limiting dilution assays in MS5 cocultures. One in 2.1 ESAM^{Hi} cells and 1 in 3.5 ESAM$^{-/Lo}$ cells gave rise to blood cells, indicating that both fractions are extremely potent sources of hematopoietic progenitors (Figure 5C left). However, we observed drastic differences between the 2 fractions regarding the frequencies of primitive progenitors with lymphopoietic potential. Whereas 1 in 8 ESAM^{Hi} cells produced CD19$^+$ B lineage cells, only 1 in 125 ESAM$^{-/Lo}$ cells were lymphopoietic under these conditions (Figure 5C right). These results suggest that primitive

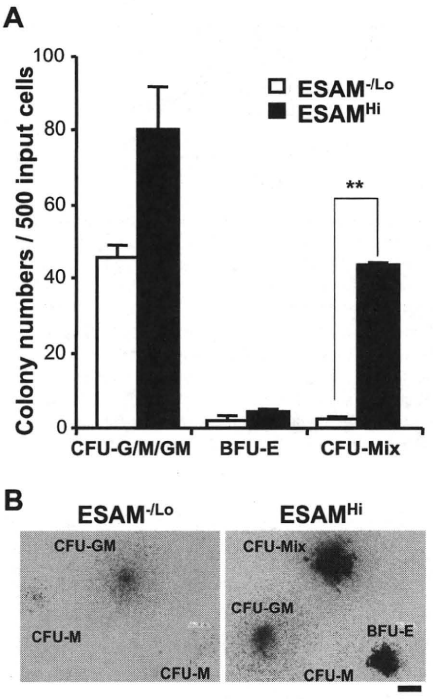

Figure 4. ESAM expression correlates with CFU activity. ESAM$^{-/Lo}$ or ESAM^{Hi} cells of the Rag1/GFP$^-$ ckit^{Hi} Sca1$^+$ fraction of E14.5 fetal liver were sorted and subjected to methylcellulose colony formation assay. Numbers of CFUs (A) and morphology of the colonies derived from the indicated CFUs (B) are shown. The results in panel A are shown as mean plus or minus SD. A black bar in panel B represents 500 mm. The data are from one of 3 independent experiments that gave similar results. Significant difference between the 2 population is indicated (**$P < .01$).

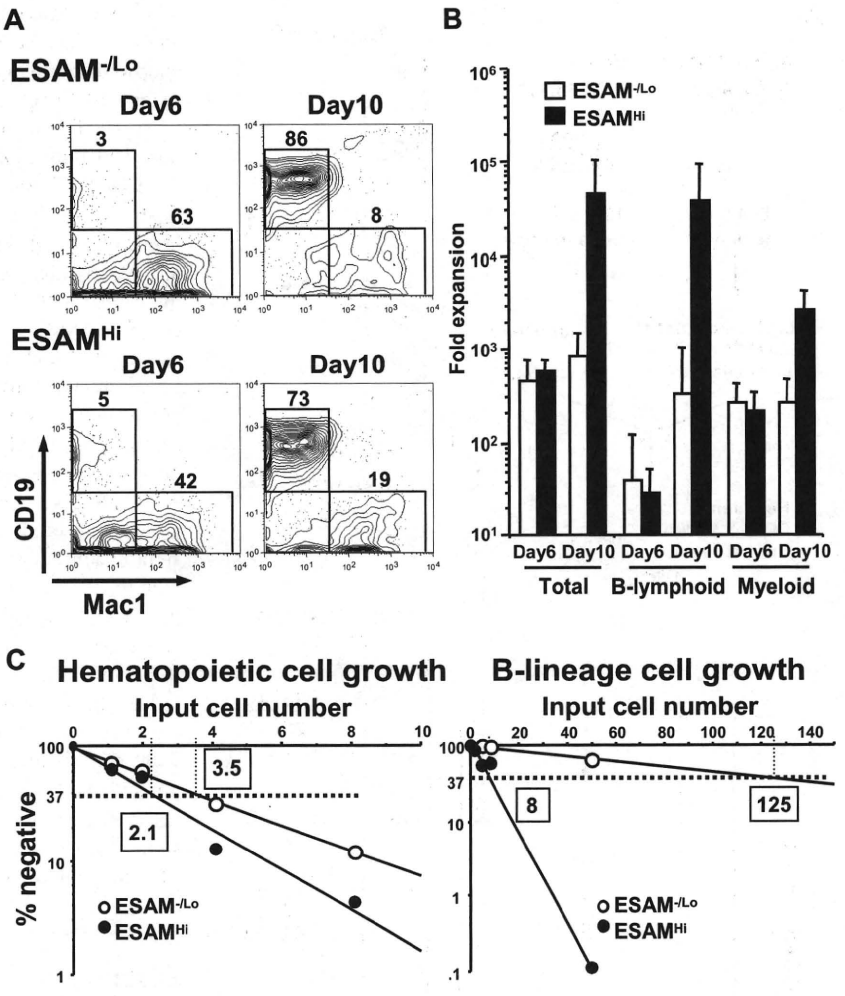

Figure 5. ESAM expression enriches primitive progenitors endowed with lymphopoietic activity. (A,B) A total of 500 ESAM$^{-/Lo}$ or ESAM^{Hi} cells of the Rag1/GFP^{-} ckit^{Hi} Sca1^{+} fraction of E14.5 fetal liver were cultured with MS5 stromal cells in the presence of SCF, Flt3-ligand, and IL-7. At the indicated period, recovered cells were counted and subjected to flow cytometry (A). Yields of total cells, CD19^{+} Mac1^{-} B-lineage cells, and Mac1^{+} CD19^{-} myeloid-lineage cells per 1 input ESAM$^{-/Lo}$ or ESAM^{Hi} progenitor were calculated and given as averages with SD bars (B). (C) Limiting dilution analyses were performed in the MS5 coculture system to determine the frequency of hematopoietic progenitors (left) and that of progenitors endowed with lymphopoietic potential (right).

stem/progenitor cells, which are multipotent for myeloid, erythroid, and lymphoid lineages, are present in the ESAM^{Hi} fraction of fetal liver.

Long-term reconstitution activity is exclusive to ESAM^{Hi} cells

To evaluate ESAM expression on long-term reconstituting HSCs in E14.5 fetal liver, we transplanted cells of the ESAM$^{-/Lo}$ or ESAM^{Hi} fraction into lethally irradiated mice (Figure 6A). Five weeks after transplantation, it was obvious that CD45.2^{+} ESAM^{Hi} cells contributed highly to the recovery of hematopoiesis in recipients, but no chimerism was detected in mice transplanted with ESAM$^{-/Lo}$ cells (Figure 6B). Indeed, although 9 of 11 mice transplanted with 1000 ESAM^{Hi} cells had clear donor CD45.2^{+} populations (> 1.0%) among peripheral leukocytes, none of 10 mice given 1000 ESAM$^{-/Lo}$ cells had evidence of chimerism. Five months after transplantation, we analyzed the contribution of CD45.2^{+} cells to long-term lymphohematopoietic reconstitution of the recipients. Although most of the 11 mice transplanted with ESAM^{Hi} cells had clear CD45.2^{+} populations in bone marrow (mean ± SD of percentage CD45.2^{+} CD45.1^{-} in total CD45^{+} cells; 16.3% ± 22.0%), none of the ESAM$^{-/Lo}$-transplanted mice contained detectable CD45.2^{+} cells in that organ (mean ± SD of percentage CD45.2^{+} CD45.1^{-} in total CD45^{+} cells; 0.02% ± 0.03%) (Figure 6C). Furthermore, multilineage recovery was observed in the bone marrow, spleen, and thymus of mice transplanted with ESAM^{Hi} cells (Figure 6D). In addition, bone marrow cells recovered from primary recipients with ESAM^{Hi} cell transplantation effectively reconstituted CD45.2^{+} lymphohematopoietic cells in secondary recipients at 5 months after transplantation (data not shown). These results indicate that high levels of ESAM expression correspond to fetal HSCs with long-term repopulating potential.

ESAM expression marks cells thought to represent HSCs in fetal and aged adult tissues

The definitive HSCs that account for lymphohematopoieisis in adults first arise in the AGM region.[28,29] To examine whether ESAM was present on those HSCs, flow cytometry analyses were performed with the Rag1/GFP^{-} cells isolated from E10.5 embryos. Tie2 and c-kit were used as additional parameters because we previously identified lymphohematopoietic cells in the early embryos as Rag1^{-} Tie2^{+} c-kit^{+}.[19] A small but conspicuous Tie2^{Hi} population was detected in E10.5 AGM cells (Figure 7A left). Interestingly, the Tie2^{Hi} AGM cells were clearly divided into 2 discrete populations according to ESAM expression (Figure 7A middle). When the 2 populations were back-plotted on the Tie2 and c-kit profile, ESAM^{+} cells were exclusively c-kit^{+} (Figure 7A right). In addition, lymphohematopoietic potential in the MS5 cocultures was highly enriched in the ESAM^{+} fraction among the Tie2^{Hi} cells. That is, the Tie2^{Hi} ESAM^{+} fraction could effectively produce both CD19^{+} lymphoid cells and Mac1^{+} myeloid cells, although the Tie2^{Hi} ESAM^{-} fraction generated only a small

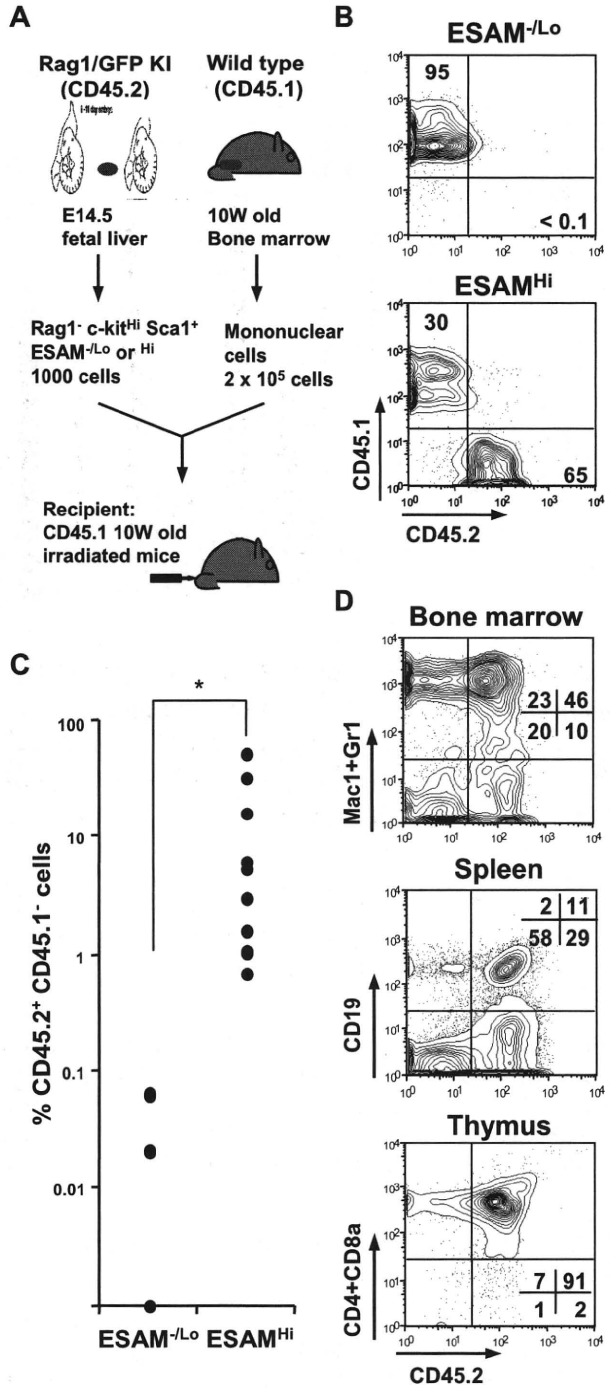

Figure 6. Long-term hematopoiesis-reconstituting activity is excusive to ESAM^{Hi} fraction. (A) The Rag1/GFP$^-$ Sca1$^+$ c-kit^{Hi} cells (CD45.2$^+$) of E14.5 fetal liver were sorted into 2 fractions, ESAM$^{-/Lo}$ and ESAM^{Hi}. Then, 1000 cells of each fraction were mixed with 2×10^5 CD45.1$^+$ whole adult bone marrow cells of 10-week-old mice and transplanted to a lethally irradiated CD45.1 mouse (A). (B) Flow cytometry analyses for peripheral leukocytes were performed at 5 weeks after transplantation. In the 2 independent experiments, 9 of 11 recipients with ESAM^{Hi} cells were clearly reconstituted by CD45.2$^+$ cells (> 1.0% in all of myeloid, T, and B lineages), whereas none of 11 recipients with ESAM$^{-/Lo}$ cells had CD45.2$^+$ cells detectable in the flow cytometry. The figure shows representative results in each group. (C,D) Twenty weeks after transplantation, all the recipients were killed, and the contribution of CD45.2$^+$ ESAM^{Hi} cells was evaluated in lymphohematopoietic organs. Percentages of CD45.2$^+$ CD45.1$^-$ population among total CD45$^+$ cells in bone marrow of each recipient were plotted (C). The long-term reconstitution of CD45.2$^+$ ESAM^{Hi} cells was confirmed with respect to myeloid, B lymphoid, or T lymphoid lineages in the bone marrow, spleen, and thymus, respectively (D).

number of Mac1$^+$ cells (Figure 7B). We concluded from these analyses that ESAM marks the primitive hematopoietic cells endowed with lymphopoietic activity in the E10.5 AGM as well as in the E14.5 liver.

A small number of Tie2^{Hi} c-kit^{Lo} ESAM^{Hi} cells were also observed among extraembryonic YS cells (Figure 7C). In addition, the E10.5 YS contained a conspicuous population whose phenotype was Tie2^{Lo} c-kit^{Hi}, and cells in that fraction expressed low levels of ESAM (Figure 7C). Cells with the same phenotype were also clearly observed in the E9.5 YS, although they were absent in the caudal half of the embryo proper (Figure S2A). These Tie2^{Lo} c-kit^{Hi} ESAM^{Lo} cells in the YS effectively produced myeloid and/or erythroid colonies in methylcellulose culture but showed little lymphopoietic potential (Figure S2B,C). Importantly, lymphopoietic activity was exclusive to the Tie2^{Hi} c-kit^{Lo} ESAM^{Hi} fraction of the PSp/AGM region, which showed no myeloid-erythroid potential in conventional methylcellulose assays.

It is well known that HSC properties change with developmental age. Indeed, Forsberg et al previously reported ESAM expression by adult marrow HSCs,[30] but the levels were weak compared with those on fetal HSCs. Therefore, we expected that ESAM, like the other endothelial antigens, would decline with HSC aging. However, we found that ESAM expression was detectable on the Rag1$^-$ LSK fraction of bone marrow through life (Figure 7D). Indeed, the proportion of ESAM^{Hi} cells and the mean fluorescence intensity of ESAM expression in the Rag1$^-$ LSK fraction increased with age (Figure 7D). Moreover, primitive myeloid-erythroid progenitors from adult bone marrow were also enriched in the ESAM^{Hi} fraction (Figure 7E). In summary, these findings demonstrate that ESAM expression is useful for exploring the biology of hematopoietic stem/progenitor cells throughout life in mice.

Discussion

We conducted gene array analyses with the principal goal of learning more about the initial differentiation of fetal HSCs to cells in lymphoid lineages. In that regard, several informative genes were identified and will be presented elsewhere (manuscript in preparation). Our screen also identified genes whose expression was previously thought to correlate with HSCs in fetal or adult tissues. Among those, *Esam* was particularly noteworthy as being drastically down-regulated during differentiation of HSCs to ELPs. We now report that it represents a potent tool for identifying HSCs over a wide range of developmental age.

ESAM was originally identified as an endothelial cell-specific protein, although it was also shown to be expressed on megakaryocytes and platelets.[22,31] A recent study also found ESAM transcripts in adult marrow HSCs when gene arrays were used to compare Thy1.1^{Lo} Flk2$^-$ LSK (long-term HSC-enriched), Thy1.1^{Lo} Flk2$^+$ LSK (short-term HSCs), and Thy1.1$^-$ Flk2$^+$ LSK (multiple progenitors).[30] We now show how ESAM levels can be exploited to obtain highly enriched CFU-Mix, lymphopoietic cells, and long-term HSCs from the Rag1$^-$ c-kit^{Hi} Sca1$^+$ fraction of E14.5 fetal liver. It is important to note that long-term HSCs in mouse embryos are unique in expressing markers, such as Flk2 and CD11b/Mac1, not characteristic of adult HSCs.[18,32] This complicates cell sorting strategies and fetal/adult comparison. We previously found that Rag1/GFP$^-$ c-kit^{Hi} Sca1$^+$ cells derived from E14.5 fetal liver reconstituted lymphohematopoiesis in lethally irradiated adults, whereas Rag1/GFP^{Lo} c-kit^{Hi} Sca1$^+$ cells transiently contributed to T and B lymphopoiesis. ESAM specific Abs can be used without